Scientia Pharmaceutica

ÖSTERREICHISCHE PHARMAZEUTISCHE GESELLSCHAFT

MDPI

Article

Phytochemical Study and Cytotoxic Properties of Hydroalcoholic Extracts of *Epilobium parviflorum* Schreb.: In Silico and In Vitro Insights

Christian Goldiș [1], Roxana Racoviceanu [2,3,*], Mihaela Jorgovan [2,3], Roxana Negrea-Ghiulai [2,3], Codruța Șoica [2,3], Alexandra Prodea [2,3], Oana Bătrîna [2,3], Gabriela Antal [2,3] and Alexandra Mioc [2,3]

[1] Faculty of Medicine, "Victor Babeș" University of Medicine and Pharmacy, 2 Eftimie Murgu Square, 300041 Timișoara, Romania; christian.goldis@student.umft.ro

[2] Faculty of Pharmacy, "Victor Babeș" University of Medicine and Pharmacy, 2 Eftimie Murgu Square, 300041 Timișoara, Romania; mihaela.coban@umft.ro (M.J.); roxana.ghiulai@umft.ro (R.N.-G.); codrutasoica@umft.ro (C.Ș.); alexandra.ulici@umft.ro (A.P.); oana.esanu@umft.ro (O.B.); gabriela.antal@umft.ro (G.A.); alexandra.mioc@umft.ro (A.M.)

[3] Research Centre for Experimental Pharmacology and Drug Design (X-Pharm Design), "Victor Babeș" University of Medicine and Pharmacy, 2 Eftimie Murgu Square, 300041 Timisoara, Romania

* Correspondence: babuta.roxana@umft.ro

Abstract

Epilobium parviflorum Schreb. is a medicinal plant used traditionally against inflammatory disorders whose cytotoxic potential is still incompletely revealed. The current study investigates the phytochemical composition and in vitro cytotoxic activity of four hydroalcoholic extracts prepared from the aerial parts of *E. parviflorum* by using maceration and Soxhlet extraction. The extracts were characterized in terms of total phenolic, flavonoid and tannins composition and LC-MS was used to identify its individual polyphenols. Their biological effects were assessed against four cancer cell lines (A375 melanoma, HT-29 colorectal adenocarcinoma, PANC-1 pancreatic carcinoma and SK-OV-3 ovarian adenocarcinoma cells), while using HaCaT keratinocytes as healthy cells in order to assess selectivity. Cell viability, cytoskeletal and nuclear morphology, mitochondrial respiration and network pharmacology were further investigated. A complex phenolic profile was revealed, with hyperoside being identified as the main component in all extracts while the extraction parameters strongly influenced the recovery of various phenolic compounds. All extracts reduced cancer cell viability in a dose-dependent manner after 24 h exposure, with the most pronounced effects observed at 720 and 1000 µg/mL, while HaCaT cells were left relatively unaffected. The morphological assessment indicated nuclear condensation, fragmentation and cytoskeletal disruption following the application of extracts. Moreover, high-resolution respirometry showed reduced oxidative phosphorylation and electron transfer system capacity thus indicating that early mitochondrial dysfunction may contribute to the cytotoxic effects. Network pharmacology revealed that ERBB2, CTNNB1, HSP90AA1 and HDAC6 might act as molecular targets in melanoma. Thus, these findings support the hypothesis that *E. parviflorum* hydroalcoholic extracts, particularly the 40% ethanol Soxhlet extract, may serve as important sources of bioactive phytocompounds with antiproliferative and apoptotic properties.

Keywords: small-flowered willowherb; phytochemical assessment; apoptosis; network pharmacology

Academic Editor: Yulin Ren

Received: 29 June 2026
Revised: 18 August 2026
Accepted: 21 August 2026
Published: 23 August 2026

1. Introduction

Natural products stand as important sources of bioactive molecules used in the development of modern drugs. Current anticancer pharmacotherapy includes various classes of synthetic drugs, such as alkylating agents, antimetabolites and targeted agents [1]. However, despite their efficiency, these agents can also act on normal cells, thus leading to a wide range of side effects such as myelosuppression, nausea, mucositis, fatigue, muscle or joint pain, skin rashes, alopecia and organ-specific toxicity [2,3]). Compared to synthetic drugs, vegetal compounds often exhibit low toxicity while acting simultaneously on multiple molecular targets, such as oxidative stress, inflammation, cell proliferation and apoptosis as well as tumor-related signaling pathways. Thus, medicinal plants continue to be investigated for the potential identification of new compounds with therapeutic potential, particularly in the field of anticancer therapy [4].

Small-flowered willowherb (*E. parviflorum*) is a biennial or perennial herbaceous plant from the Onagraceae family. It grows in wetlands such as lakes or rivers all throughout Europe, Asia, Africa and North America [5,6].

The aerial parts of *E. parviflorum*, such as its stems, leaves and flowers, have been long used for medical purposes as infusions or extracts aimed to alleviate kidney and urinary tract disorders, inflammatory conditions, gastric ulcers and gastritis as well as respiratory diseases, including asthma and whooping cough. Also, pharmaceutical formulations containing extracts of *E. parviflorum* have been traditionally used to manage diarrhea, prostate disorders and conditions related to hormonal imbalance [7].

The interest raised by *E. parviflorum* extracts is mainly caused by its rich phytochemical composition, consisting in polyphenols, sterols (i.e., β-sitosterol), triterpenes, fatty acids, flavonoids (i.e., myricetin, kaempferol, catechin, quercetin-3-*O*-β-D-glucuronide) as well as tannins (i.e., oenothein B) [8]. Consequently, *E. parviflorum* exerts antioxidant, anti-inflammatory and cytotoxic effects [7]; as an example, *E. parviflorum* extracts are able to reduce the activity of cyclooxygenase enzymes COX-1 and COX-2 involved in inflammatory processes. The cytotoxic potential of *E. parviflorum* has been investigated in various tumor models; as an example, previous studies have shown that extracts obtained from *Epilobium* species, including *E. parviflorum*, are able to inhibit the proliferation of hormone-dependent prostate cancer cells by inducing apoptosis through the activation of mitochondrial pathways [9]. In colorectal cancer, the aqueous and ethanolic extracts of *E. parviflorum* reduced the viability of HT-29 cells in a dose-dependent manner and triggered apoptotic events such as the stimulation of caspase-3 and caspase-8 as well as nuclear fragmentation [10]. Antiproliferative effects have also been reported in MCF-7 breast cancer cells whose growth was inhibited by *E. parviflorum* extracts, with methanolic extracts exhibiting stronger cytotoxic activity compared to their respective aqueous counterparts [11]. More recently, the cytotoxic potential of *E. parviflorum* was reported in human A375 and COLO-679 malignant melanoma cells where its methanolic extract reduced cell viability in a time- and concentration-dependent manner while leaving healthy HaCaT keratinocytes relatively unaffected [6]. Nevertheless, the available evidence is fragmented across individual cancer models and provides a limited view regarding the mechanisms underlying the observed cytotoxicity. Therefore, a broader and integrated evaluation of its phytochemical profile and biological activity is needed.

The assessment of *E. parviflorum* as a cytotoxic agent is particularly relevant since inflammation, oxidative stress, uncontrolled proliferation and apoptosis resistance are commonly involved in tumor initiation and progression as well as the development of treatment resistance. Being rich in polyphenols and ellagitannins, the plant extracts may therefore be used for the identification of compounds able to simultaneously interfere with several cancer-related mechanisms [12,13]. However, despite the available data regarding

its activity in selected cancer cell lines, the cytotoxic potential of *E. parviflorum* remains incompletely investigated, particularly in tumor types displaying distinct biological traits that pose therapeutic challenges.

The choice of melanoma, colorectal, pancreatic and ovarian cancer cells as targets for the currently investigated extracts is supported by their biological and clinical relevance. According to recent global cancer reports, colorectal cancer remains one of the most frequently diagnosed malignant pathologies worldwide while pancreatic cancer is generally associated with poor prognosis combined with limited therapeutic options; ovarian cancer stands as a major gynecological malignancy often diagnosed in advanced stages while melanoma is the most aggressive type of skin cancer with high metastatic potential [14]. Therefore, the screening of natural extracts against this range of cancer cell lines may provide useful information regarding their potential spectrum of cytotoxic effects and anticancer potential. Notably, although the cytotoxic effects of *E. parviflorum* have been investigated in several cancer cell lines, including HT-29 and A375 cells [6,10], to the best of our knowledge, the effects against SK-OV 3 and PANC-1 cell lines have not been previously reported.

Taking into account the emerging evidence regarding the antiproliferative and pro-apoptotic properties of *E. parviflorum* presumably caused by its rich content in polyphenols and ellagitannins, the present study aimed to assess its phytochemical composition and cytotoxic effects in A375 human melanoma, HT-29 colorectal adenocarcinoma, PANC-1 pancreatic carcinoma and SK-OV-3 ovarian adenocarcinoma cells and to evaluate the safety and selectivity in healthy human HaCaT keratinocytes. In addition, high-resolution respirometry was used to investigate whether the observed cytotoxic effects were correlated with mitochondrial respiratory alterations. Furthermore, an in silico network pharmacology analysis was performed to identify the potential molecular targets and the pathways relevant to melanoma. Therefore, the objective of this study is to provide a broader and integrated assessment of *E. parviflorum* extracts by combining the phytochemical characterization with biological and computational approaches, while also extending the investigation, to the best of our knowledge, to additional tumor models that were not previously investigated in this context.

2. Materials and Methods

2.1. Chemicals, Reagents, Standards and Equipment

Ethanol, methanol and acetic acid of 99.9% purity were purchased from Merck (Darmstadt, Germany). Folin-Ciocâlteu reagent, gallic acid, sodium carbonate, quercetin, aluminum chloride, potassium acetate, catechin, vanillin and concentrated hydrochloric acid were purchased from Sigma-Aldrich Chemie GmbH (Taufkirchen, Germany). The phenolic components reference standards for LC-MS, including rosmarinic acid, caftaric acid, gentisic acid, chlorogenic acid, caffeic acid, p-coumaric acid, ferulic acid and sinapic acid, hyperoside, isoquercitrin, rutin, myricetin, fisetin, quercitrin, quercetol, luteolin, kaempferol, and apigenin, were also purchased from Sigma-Aldrich Chemie GmbH (Taufkirchen, Germany). For the preparation of sample solutions ultrapure deionized water was provided by a MiliQ system Milli-Q® Integral Water Purification System (Merckmilipore, Darmstadt, Germany).

General equipment used during the experimental procedures included a Shimadzu UV-1900i UV-Vis spectrophotometer (Shimadzu Corporation, Kyoto, Japan) operating within the wavelength range of 400–800 nm, a rotary evaporator (Heidolph Instruments GmbH & Co. KG, Schwabach, Germany), an electrical grinder (Bosch TSM6A013B, BSH Hausgeräte GmbH, Munich, Germany), a Soxhlet installation (DWK Life Sciences, Wertheim, Germany), a Buchner funnel (DWK Life Sciences, Wertheim, Germany), a vacuum filtration system (Vacuubrand GmbH + Co. KG, Wertheim, Germany) and a vortex mixer (IKA-Werke GmbH & Co. KG, Staufen im Breisgau, Germany).

2.2. Plant Material and Extract Preparation

The dried aerial parts of *E. parviflorum* (stems, leaves, flowers) were purchased from Fares, Romania. The plant material was supplied in packages of 50 g each and registered under 20/25 and 22/25 lot numbers. Prior to extraction, the plant material was mechanically pulverized using an electrical grinder. Two extraction methods were employed: (1) maceration at room temperature (10 days) in the dark, and (2) Soxhlet extraction (15 full cycles). Two solvent mixtures were used in each case: 40% and 60% (*v*/*v*) hydroalcoholic mixtures prepared with absolute ethanol and distilled water. The vegetal material to solvent ratio was 1:10 (*w*/*v*) in the maceration procedure and 1:13 (*w*/*v*) in the Soxhlet extraction. Following extraction, the macerated samples E1 and E2 were separated through vacuum filtration using a Buchner funnel fitted with filter paper. The Soxhlet extracts, E3 and E4 were collected from the extraction flask. Then, the solvent was removed from all extracts under reduced pressure using a rotary evaporator, at 60 °C. The final dry extract was stored in the dark at 4 °C until further processing. Table 1 displays sample codes, extraction methods, solvents and extraction yields.

Table 1. Extraction condition and yield.

Sample Code	Extraction Method	Solvent	Yield
E1	Maceration in dark (10 days)	40% ethanol	18.00%
E2	Maceration in dark (10 days)	60% ethanol	15.58%
E3	Soxhlet (15 full cycles)	40% ethanol	18.22%
E4	Soxhlet (15 full cycles)	60% ethanol	15.76%

2.3. Analysis by High-Performance Liquid Chromatography Coupled with Mass Spectrometry (LC-MS)

High performance liquid chromatography (HPLC/LC) coupled with mass spectrometry (MS) experiments were conducted on a 6120 LC-MS analytical system from Agilent (Santa Clara, CA, USA) consisting of 1260 Infinity HPLC equipped with G1322A degasser, G1311B quaternary pump, G1316A column thermostat, G1365C MWD detector, G7129A autosampler coupled with a Quadrupolar (Q) mass spectrometer equipped with electrospray ionization source (ESI). LC-MS is connected to a PC computer running the OpenLAB CDS ChemStation Workstation software, version C.01.08 to control the instrument, acquire and process LC-MS data.

Quantification of phenolic components in small-flowered willowherb extract samples E1–E4 was conducted by LC-MS. phenolic components were separated on a reverse phase Zorbax Eclipse Plus C18 column (3.0 × 100 mm × 3.5 µ) by an LC-MS method that enabled the screening and quantification of analyzed extracts for 18 polyphenols, such as: rosmarinic acid, caftaric acid, gentisic acid, chlorogenic acid, caffeic acid, p-coumaric acid, ferulic acid and sinapic acid, hyperoside, isoquercitrin, rutin, myricetin, fisetin, quercitrin, quercetol, luteolin, kaempferol and apigenin, as described before [15,16]. Polyphenols were screened in gradient elution with a mobile phase that consists of a mixture of 0.1% acetic acid solution and methanol as follows: 5 min 5% methanol, up to 38 min in gradient elution reaching 42% methanol and 5% methanol up to 42 min. The elution of all components was achieved in about 40 min at a flow rate of 1 mL/min, injection volume 10 µL and column temperature of 40 °C. UV detection of polyphenols was conducted at 330 and 370 nm. MS detection was achieved by electrospray ionization (ESI) in the negative ion mode using single ion monitoring (SIM) which enabled the simultaneous screening and quantification of all 18 screened compounds. MS parameters: capillary voltage 3500 V, dry gas flow 12 L/min at 350 °C, nebulizer pressure 55 psig and fragmentor at 70. For the quantification of phytocompounds in the extracts, calibration curves were conducted

by the external standard method in the 0.05–2 µg/mL range, for a six-point plot for each compound [17]. The m/z scale of the mass spectrum was calibrated by use of an external calibration standard ESI Tuning Mix from Agilent (Santa Clara, CA, USA).

All dry extract samples were dissolved in pure methanol, homogenized with a WisdVM-10vortex mixer (Witeg Labortechnik GmbH, Wertheim, Germany) and centrifuged for 2 min at 10,000 rpm in a ThermoMicro CL17microcentrifuge (Thermo Fisher Scientific, MA, USA). The supernatant was collected and submitted to LC-MS analysis.

2.4. Spectrophotometric Phytochemical Assay

Absorbance measurements for the spectrophotometric assays were performed using a Shimadzu UV-1900i UV-Vis spectrophotometer.

2.4.1. The Total Phenolic Content (TPC)

TPC was determined using the Folin-Ciocâlteu assay, following a slightly modified colorimetric method [18]. Briefly, 0.5 mL of gallic acid standard solution or extract solution was mixed with 2.5 mL of Folin-Ciocâlteu reagent previously diluted 1:10 with distilled water and was left to rest for 5 min at 25 °C. Then, 2.0 mL of Na_2CO_3 of concentration 7.5% was added in the mixture, the samples were vigorously vortexed and incubated for 30 min at 25 °C, in the dark. The next step was the measuring of the absorbance at 765 nm wavelength against the blank. In addition, considering the slightly colored samples a correction of the absorbance was performed. Initially, separate gallic acid calibration curves were registered in the two used solvents 40% ethanol and 60% ethanol in order to evaluate the possible influence of the solvent composition. As the two curves showed comparable linearity and regression parameters, the same calibration equation was considered suitable for calculating the total phenolic content of all extracts. TPC was expressed as mg gallic acid equivalents per g dry extract.

2.4.2. Total Flavonoid Content (TFC)

TFC was calculated using the quercetin standard and the method previously reported by Chang et al. [19] a with few minor modifications. Basically, at 0.5 mL extract solution or quercetin standard solution were added 1.5 mL of ethanol, 0.1 mL $AlCl_3$ of concentration 10%, 0.1 mL CH_3COOK 1M and 2.8 mL H_2O were added. The resulting mixture was strongly vortexed and incubated for 30 min at 25 °C, in the dark. Afterwards, the absorbance was measured at 415 nm against the blank. Similar to the TPC determination, a correction of the absorbance was also applied in this case. To avoid solvent–induced differences in absorbance values, the quercetin and the dry extracts were solubilized in 80% ethanol. TFC was expressed as mg quercetin equivalents per g dry extract.

2.4.3. Condensed Tannin Content (CTC)

CTC was determined using the acidified vanillin method, based on the original version [20] and recently described by Géorcelin et al. [21]. In summary, 0.5 mL extract solution or cathechin standard solution was mixed with 3.0 mL vanillin 4% in methanol and 1.5 mL concentrated HCl. The mixture was strongly vortexed and incubated for 15 min at 25 °C, in the dark. Then, the value of the absorbance was measured at 500 nm against the blank. As in the previous assays, a correction of the absorbance was performed. Cathechin and the dry extracts were dissolved in 80% ethanol for consistency and to prevent solvent-induced variations in absorbance. CTC was expressed as mg catechin equivalents per g dry extract.

2.5. Cell Culture

The cell lines used in this study were human immortalized keratinocytes (HaCaT), human melanoma cells (A375), human colorectal adenocarcinoma cells (HT-29), human

pancreatic adenocarcinoma cells (PANC-1), and human ovarian adenocarcinoma cells (SK-OV-3). HaCaT cells were obtained from CLS Cell Lines Service GmbH (Eppelheim, Germany), whereas A375, HT-29, PANC-1, and SK-OV-3 cell lines were purchased from the American Type Culture Collection (ATCC, Lomianki, Poland). Cells were received as frozen stocks and stored in liquid nitrogen until use. HaCaT, A375, and PANC-1 cells were cultured in high-glucose Dulbecco's Modified Eagle Medium (DMEM) supplemented with 10% fetal bovine serum (FBS) and 1% penicillin–streptomycin solution. HT-29 and SK-OV-3 cells were maintained in McCoy's 5A medium supplemented with 10% FBS and 1% penicillin–streptomycin solution. All cell lines were maintained in a humidified atmosphere containing 5% CO_2 at 37 °C.

2.6. Cell Viability Assay

The Alamar Blue colorimetric assay was used to evaluate the cell viability of HaCaT, A375, HT-29, PANC-1, and SKOV cell lines after 24 h of stimulation with 3.6 µg/mL, 36 µg/mL, 360 µg/mL, 720 µg/mL, and 1000 µg/mL E1–E4. Cells (1×10^4/well) were seeded in 96-well plates and incubated at 37 °C and 5% CO_2 until reaching 80–85% confluency. The anticancer drug 5-Fluorouracil (5-FU) was used as a positive control. The 5-FU stock solution (10 mM) was prepared in ultrapure distilled water and further diluted in culture media to the final concentrations of 1, 10, 25, 50 and 100 µM for 24 h. The dried E1–E4 extracts were dissolved in DMSO to obtain 200 mg/mL stock solutions, which were then vortexed and sonicated until complete dissolution. The stock solutions were diluted with culture medium to the required concentrations; the final concentration of DMSO used in the control and experimental wells was 0.5% (*v*/*v*), a concentration at which DMSO does not influence cell viability. After 24 h, the cells were counterstained with 0.01% Alamar Blue and incubated for an additional 3 h. The fluorescent signal was recorded using a Synergy HTX multi-mode microplate reader (BioTek Instruments, Inc., Winooski, VT, USA), with excitation at 528 nm and emission at 590 nm. Each experiment was performed in triplicate.

2.7. Immunofluorescence Assay

Immunofluorescence staining was performed to evaluate cytoskeletal organization and nuclear morphology. Cells (2×10^5 cells/well) were seeded in 12-well plates and cultured until reaching 80–85% confluence. Subsequently, cells were treated for 24 h with 360 µg/mL E1–E4. After treatment, cells were washed with PBS, fixed with 4% paraformaldehyde for 10 min, and permeabilized using 0.1% Triton X-100 for 15 min. Non-specific binding sites were blocked with 3% BSA for 30 min. Cells were then incubated for 1 h at room temperature with a mouse monoclonal anti-β-actin antibody (Product #MA1-140, Thermo Fisher Scientific, Inc., Waltham, MA, USA; 1:2000), followed by incubation with Alexa Fluor Plus 488-conjugated goat anti-mouse IgG (H+L) secondary antibody (Product #A32723, Thermo Fisher Scientific, Inc., Waltham, MA, USA; 1:500) for 30 min in the dark. Nuclei were counterstained with Hoechst 33342 (Product #62249, Thermo Fisher Scientific, Inc., Waltham, MA, USA, 1:2000) for 10 min in the dark. Samples were subsequently visualized using a Thermo Scientific EVOS™ M5000 Imaging System (Thermo Fisher Scientific, Inc., Waltham, MA, USA); the images were analyzed with a 40× objective to assess cytoskeletal integrity and nuclear morphology.

2.8. High-Resolution Respirometry

Mitochondrial respiratory function was assessed by high-resolution respirometry using an Oxygraph-2k system (Oroboros Instruments, Innsbruck, Austria). The experiments were performed at 37 °C after the calibration process. For the respirometric assay, cells were cultured in T75 cm^2 flasks until reaching 85% confluency. Following tripsinizations, the cells (2×10^6 cells/chamber) were suspended in mitochondrial respiration medium

MIRO5 (110 mM D-sucrose, 20 mM taurine, 0.5 mM EGTA, 20 mM HEPES, 3 mM $MgCl_2$, 60 mM lactobionic acid, 10 mM KH_2PO_4 and 1 g/L bovine serum albumin; pH was adjusted to 7.1 using KOH). Oxygen flux was recorded using DatLab software 8.2 software. Mitochondrial respiration was assessed following a substrate–uncoupler–inhibitor titration protocol, as previously described [22]. E1 and E3 were added to the chamber prior to the experiment; in order to investigate the early mitochondrial responses without inducing extensive cell death, the concentration selected, 360 µg/mL, was below the calculated IC_{50}. Briefly, after 10 min of equilibration (routine respiration), the cell membrane was permeabilized using digitonin (1 µg/L × 10^6 platelets). Complex I-linked respiration was assessed after the addition of glutamate (5 mM) and malate (5 mM, State 2CI), followed by ADP (1 mM) addition to stimulate oxidative phosphorylation through complex I (OXPHOSCI). Subsequently, succinate (10 mM), a complex II substrate, was added to measure the maximal OXPHOS supported by convergent electron input through complexes I and II (OXPHOSCI+II). Oligomycin (1 µg/mL) was then added to inhibit complex V, ATP synthase and to measure the non-phosphorylating respiration state (State 4CI+II). The maximal capacity of the electron transport system (ETS) was evaluated by a stepwise titration of FCCP (1 µM/step) until reaching the maximal uncoupled respiration (ETSCI+II). Rotenone (2 µM) was added to inhibit complex I and to measure the complex II-supported electron transport capacity (ETSCII). In the final step of the protocol, antimycin A (1 µg/mL) was added to inhibit complex III and to measure the residual oxygen consumption.

2.9. Statistical Analysis

The cell viability results were analyzed using one-way analysis of variance (ANOVA), followed by Dunnett's multiple comparisons test. For the high-resolution respirometry studies, the statistical differences vs. control were determined using two-way ANOVA with Bonferroni's multiple comparison post-test. Values were considered to be statistically significant if $p < 0.05$ (* $p < 0.05$; ** $p < 0.01$; *** $p < 0.001$ vs. control cells).

2.10. Target Prediction and Network Pharmacology

2.10.1. Melanoma-Related Gene Selection

The top 300 protein-coding genes based on their relevance score for melanoma in Homo sapiens were retrieved from the GeneCards database [23]. Furthermore, the genes were converted into their corresponding protein-coding entries through the UniProt database [24].

2.10.2. Ligand Selection and Preparation

Five compounds were selected for the network pharmacology analysis: caftaric acid [25], quercetin [26], myricetin [27], ellagic acid [28] and gallic acid [29]. The 3D structures of the selected compounds were downloaded from PubChem v 4.1 [30], and then imported into Avogadro (v. 2.0) [31], where geometric optimization was performed under the MMFF94 force field to ensure a relevant 3D conformation.

2.10.3. Reverse Pharmacophore Mapping

The optimized 3D structures of the compounds were imported into the PharmMapper server [32] to identify potential protein targets for the selected compounds. Drugable pharmacophore models were selected as the target set and the maximum number of targets identified was limited to 300. Additionally, to minimize discrepancies and ensure consistency across the various databases used, we retrieved the UniProt IDs from the UniProt database [24]. The intersection of the targets identified for the selected compounds with the proteins encoded by genes relevant for melanoma was made using the Interactivenn web tool [33].

2.10.4. Protein–Protein Interaction, Network Construction and Functional Enrichment Analysis

The protein targets of compounds relevant to melanoma were imported into the STRING database [34] to identify interactions in Homo sapiens. The resulting STRING data was then imported into Cytoscape (v3.10.4) [35] to construct a protein–protein interaction network, further used to analyze the degree, betweenness centrality, and closeness centrality of the nodes. Furthermore, a custom functional enrichment analysis was performed in Metascape v3.5.20260701 [36] using the KEGG Pathway, GO Biological Processes, and Wiki pathways as source databases to identify biologically relevant pathways in which these targets are found.

2.11. Molecular Docking

Molecular docking was performed to investigate the potential interactions of quercetin and ellagic acid with the four top-ranked protein targets identified by the network topological analysis, namely ERBB2, CTNNB1, HSP90AA1 and HDAC6. The crystal structures of human ERBB2 (PDB ID: 3PP0), CTNNB1 (PDB ID: 7AFW), HSP90AA1 (PDB ID: 6LR9) and HDAC6 (PDB ID: 5EDU) were retrieved from the RCSB Protein Data Bank. Prior to docking, the co-crystallized ligands, water molecules and other non-protein components were removed from the receptor structures using PyMOL v 3.1. Molecular docking simulations were performed using AutoDock Vina v1.2.x implemented in PyRx version 0.8. The binding sites were defined based on the positions of the respective co-crystallized ligands. The grid centers (x, y, z) were 16.906, 17.389, and 25.824 Å for ERBB2; 60.714, −40.567, and 17.955 Å for CTNNB1; 2.711, 35.559, and 23.507 Å for HSP90AA1; and 9.973, −47.820, and 103.754 Å for HDAC6. The corresponding grid dimensions were 12.427 × 19.309 × 11.445 Å, 14.116 × 9.510 × 8.806 Å, 15.244 × 16.134 × 12.018 Å, and 25.000 × 21.131 × 25.000 Å, respectively. An exhaustiveness value of 8 was used for all docking calculations. For each ligand–target complex, the pose with the lowest predicted binding energy was selected for subsequent interaction analysis. The selected docking poses and their protein–ligand interactions were analyzed and visualized using BIOVIA Discovery Studio Visualizer 2024 (Dassault Systèmes, San Diego, CA, USA).

3. Results

3.1. Phytochemical Characterization

3.1.1. LC-MS Phenolic Components Profile

Small-flowered willowherb alcoholic extracts E1–E4 were subjected to LC-MS and analyzed under identical solution and instrumental conditions. Obtained results revealed the identification/quantification, according to their Rt and m/z values, of a total of 15 polyphenols in E1–E4 extracts, with some differences in terms of their quantification in each extract (Table 2). The identified phytocompounds fall into polyphenolic acid groups including cinnamic acid derivatives, flavonoids, flavones and flavonols. Following their elution intervals, identified phytocompounds were: caftaric acid, gentisic acid, chlorogenic acid, caffeic acid, p-coumaric acid, ferulic acid, hyperoside, isoquercitrin, rutin, myricetin, fisetin, quercitrin, quercetol, luteolin, and apigenin, expressed as μg/mg dry extract (d.e.)

The most abundant phenolic components identified in the extracts was hyperoside, as dominant polyphenol, accompanied by smaller concentrations of caftaric acid, gentisic acid, myricetin and quercitrin. LC-MS results revealed also the presence of other compounds that were identified, some of them in trace amounts, falling below the limit of quantification in some cases., such as chlorogenic acid, caffeic acid, p-coumaric acid, ferulic acid, isoquercitrin, rutin, myricetin, fisetin, quercitrin, quercetol, luteolin, and apigenin.

Table 2. Polyphenolic profile of Small-flowered willowherb extracts samples E1, E2, E3 and E4 analyzed by LC-MS.

No.	Compound Name	Rt (min)	$[M\text{-}H^+]^+$ (*m*/*z*)	E1 (µg/mg d.e.)	E2 (µg/mg d.e.)	E3 (µg/mg d.e.)	E4 (µg/mg d.e.)
1.	Caftaric acid	1.96	311	2.60	2.97	2.38	2.4
2.	Gentisic acid	2.67	153	0.83	0.54	0.38	0.35
3.	Chlorogenic acid	6.45	353	<LOQ	<LOQ	<LOQ	0.86
4.	Caffeic acid	6.97	179	0.3	<LOQ	<LOQ	<LOQ
5.	P-coumaric acid	10.56	163	1.17	<LOQ	0.35	0.8
6.	Ferulic acid	13.91	193	ND	ND	ND	<LOQ
7.	Hyperoside	21.56	463	26.49	24.84	25.12	24.28
8.	Isoquercitrin	22.50	463	<LOQ	0.92	2.07	2.10
9.	Rutin	23.01	609	ND	<LOQ	<LOQ	<LOQ
10.	Myricetin	24.29	317	13.03	3.13	<LOQ	<LOQ
11.	Fisetin	25.68	285	ND	ND	ND	<LOQ
12.	Quercitrin	26.18	447	2.3	2.28	1.65	2.26
13.	Quercetol	30.38	301	2.66	<LOQ	<LOQ	ND
14.	Luteolin	32.78	285	0.33	<LOQ	<LOQ	<LOQ
15.	Apigenin	36.91	269	0.11	<LOQ	<LOQ	<LOQ

Notes: ND—not detected, below the limit of detection; <LOQ—not quantified, below the limit of quantification.

LC-MS analysis indicated similar results for all extracts in terms of polyphenols concentrations and expression, with some differences regarding some phytocompounds such as, myricetin, quercetol or isoquercitrin. The presence of the dominant compound, hyperoside respectively, was almost equivalent in the E1–E4 extracts. The richest extract consistent with the concentration of identified compounds was E1, while E2–E4 expressed similar amounts of phytocompounds.

3.1.2. Total Phenolic Content

The total phenolic content (TPC) of the four *E. parviflorum* extracts was determined using the Folin–Ciocalteu assay and expressed as mg gallic acid equivalents per gram of dry extract (mg GAE/g extract). Preliminary experiments were performed for concentrations ranging between 25 and 500 µg/mL. The method was performed with an extract concentration of 200 µg/mL, which ensured absorbance values within the linear range of the calibration curve. Gallic acid calibration curve was linear over the concentration range of 0–200 µg/mL, with the regression equation $y = 0.0101x + 0.0059$ and $R^2 = 0.9990$. The test was performed in triplicate and the results were reported as mean value ± standard deviation (SD) in Table 3.

Table 3. Total phenolic content of the analyzed extracts.

Extract	Corrected Abs	GAE from Curve	TPC
E1	0.593 ± 0.002	58.13 ± 0.20 µg/mL	290.6 ± 1.0 mg GAE/g extract
E2	1.151 ± 0.005	113.41 ± 0.45 µg/mL	567.0 ± 2.2 mg GAE/g extract
E3	0.574 ± 0.002	56.25 ± 0.20 µg/mL	281.2 ± 1.0 mg GAE/g extract
E4	1.006 ± 0.003	99.02 ± 0.30 µg/mL	495.1 ± 1.5 mg GAE/g extract

In this study, the TPC values ranged from 281.2 ± 1.0 to 567.0 ± 2.2 mg GAE/g extract. Among the analyzed samples, E2 showed the highest TPC value, followed by E4, E1 and E3. E2 and E4, the extracts performed with ethanol 60%, showed higher TPC values, with 567.0 ± 2.2 and 495.1 ± 1.5 mg GAE/g extract, respectively. The 40% ethanol extracts, E1

and E3, showed significantly lower values of 290.6 ± 1.0 and 281.2 ± 1.0 mg GAE/g extract, respectively. Thus, the decreasing order of TPC was E2 > E4 > E1 > E3.

3.1.3. Total Flavonoid Content

The total flavonoid content (TFC) was determined using the aluminum chloride colorimetric assay and was expressed as mg quercetin equivalents per gram of dry extract (mg QE/g extract). Preliminary tests were performed for a concentration range of 200–3000 µg/mL. The assay was performed at an extract concentration of 2000 µg/mL, that was selected because this concentration provided absorbance values within the linear range of the calibration curve. The quercetin calibration curve showed excellent linearity over the concentration range of 0–200 µg/mL, with the regression equation y = 0.0066x + 0.0065 and R^2 = 0.9995. The test was performed in triplicate and the results were reported as mean value ± standard deviation (SD) in Table 4.

Table 4. Total flavonoid content of the analyzed extracts.

Extract	Corrected Abs	QE from Curve	TFC
E1	0.196 ± 0.001	28.71 ± 0.15 µg/mL	14.36 ± 0.08 mg QE/g extract
E2	0.301 ± 0.002	44.62 ± 0.30 µg/mL	22.31 ± 0.15 mg QE/g extract
E3	0.243 ± 0.001	35.83 ± 0.15 µg/mL	17.92 ± 0.08 mg QE/g extract
E4	0.286 ± 0.002	42.30 ± 0.23 µg/mL	21.15 ± 0.12 mg QE/g extract

For the analyzed extracts, the TFC values ranged from 14.36 ± 0.08 to 22.31 ± 0.15 mg QE/g extract. E2 proved the highest flavonoid content, namely 22.31 ± 0.15 mg QE/g extract, followed by E4, with 21.15 ± 0.12 mg QE/g extract. Lower values were obtained for E3 and E1, with 17.92 ± 0.08 and 14.36 ± 0.08 mg QE/g extract, respectively. The decreasing order of TFC was therefore E2 > E4 > E3 > E1. Similar to the TPC results, the 60% ethanol extracts displayed higher flavonoid contents than the corresponding 40% ethanol extracts.

3.1.4. Condensed Tannin Content

Condensed tannin content (CTC) was determined using the vanillin–HCl method and expressed as mg catechin equivalents per gram of dry extract (mg CE/g extract). Preliminary tests were performed for a concentration range of 500–5000 µg/mL. The assay was performed at an extract concentration of 4000 µg/mL, which provided absorbance values within the catechin calibration range. The catechin calibration curve showed excellent linearity over the concentration range of 0–200 µg/mL, with the regression equation y = 0.0028x − 0.0061 and R^2 = 0.9996. The test was performed in triplicate and the results were reported as mean value ± standard deviation (SD) in Table 5.

Table 5. Condensed tannin content of the analyzed extracts.

Extract	Corrected Abs	CE from Curve	CTC
E1	0.1003 ± 0.0006	38.01 ± 0.21 µg/mL	9.50 ± 0.05 mg CE/g extract
E2	0.0917 ± 0.0006	34.92 ± 0.21 µg/mL	8.73 ± 0.05 mg CE/g extract
E3	0.124 ± 0.0010	46.46 ± 0.36 µg/mL	11.62 ± 0.09 mg CE/g extract
E4	0.125 ± 0.0010	46.82 ± 0.36 µg/mL	11.71 ± 0.09 mg CE/g extract

The extracts showed CTC values that varied from 8.73 ± 0.05 to 11.62 ± 0.09 mg CE/g extract. Extracts E4 and E3 presented the highest condensed tannin contents, with 11.71 ± 0.09 and 11.62 ± 0.09 mg CE/g extract, respectively. E1 showed an intermediate value of 9.50 ± 0.05 mg CE/g extract, while E2 showed the lowest value, 8.73 ± 0.05 mg

CE/g extract. The decreasing order of CTC was therefore E4 ≈ E3 > E1 > E2. In contrast to TPC and TFC, the condensed tannin content did not follow the same extract ranking, indicating that the catechin-reactive condensed tannin fraction varied independently from the global Folin-reactive phenolic content.

3.1.5. Comparative Phytochemical Overview of the Extracts

Overall, the spectrophotometric assays revealed that the 60% ethanol extracts, especially E2 and E4, were richer in total phenolic and flavonoid compounds than the 40% ethanol extracts. However, this pattern was not observed for condensed tannins, for which the Soxhlet extracts, particularly E3 and E4, showed the highest values.

Interestingly, the LC-MS profile indicated E1 as the richest extract in terms of quantified targeted polyphenols, mainly due to its higher levels of myricetin and quercetol. In contrast, the global spectrophotometric assays indicated E2 as the richest extract in total phenolic and flavonoid content. This apparent difference may be explained by the fact that LC-MS quantified only selected individual compounds, whereas the Folin–Ciocâlteu and aluminum chloride assays estimate broader classes of reducing phenolic compounds and flavonoid-like molecules. Therefore, the chemical characterization suggests that extraction solvent and method influenced not only the total amount of phytochemicals, but also the relative distribution of different phenolic subclasses.

3.2. Epilobium parviflorum Effect on Cell Viability

The results obtained after the assessment of cell viability revealed that, after 24 h treatment, all four extracts (E1–E4) induced a concentration-dependent cytotoxic effect across all the tested cell lines. Overall, the decrease in cell viability was statistically significant starting at 360 µg/mL, with the strongest effects being observed at 720 and 1000 µg/mL.

In the HaCaT cell line all the extracts induced a dose-dependent decrease in viability; however, the observed reduction was generally moderate compared to the effects on the cancer cell lines. Statistical significance was obtained for all extracts only at the highest treatment doses (720 and 1000 µg/mL), as follows: 69.55% ± 9.0 (1000 µg/mL E1), 76.36% ± 6.3 and 70.96% ± 3.7 (720 and 1000 µg/mL E2), 74.09% ± 4.3 (1000 µg/mL E3) and 80.75% ± 4.4 (1000 µg/mL E4) vs. the positive control, 5- FU (35.88% ± 4.0) and vs. the control (100%) (Figure 1A–C).

In A375 melanoma cells, all extracts decreased cell viability in a concentration-dependent manner, with the most pronounced effects observed at intermediate and high concentrations (360–1000 µg/mL). E3 induced the strongest antiproliferative activity starting at 36 µg/mL: 64.13% ± 8.4 (36 µg/mL), 55.69% ± 7.9 (360 µg/mL), 45.10% ± 4.6 (720 µg/mL) and 28.01% ± 7.26 (1000 µg/mL). E1 and E4 also strongly decreased cell viability, as follows: 57.18% ± 4.9 (360 µg/mL), 49.96% ± 10.1 (720 µg/mL) and 35.41% ± 11.8 (1000 µg/mL)—E1 and 61.17% ± 9.1 (360 µg/mL), 54.12% ± 6.7 (720 µg/mL) and 46.92% ± 4.0 (1000 µg/mL)—E4 vs. 19.65% ± 3.6 5-FU (100 µM) and vs. control (100%) (Figure 1D–F).

All four extracts (E1–E4) induced a clear dose-dependent decrease in PANC-1 cell viability, but the intensity of the effect differed between extracts. The strongest antiproliferative effect was again observed for E3. Cell viability decreased to 77.37% ± 9.5 (36 µg/mL), 65.04% ± 4.8 (360 µg/mL), 49.93% ± 4.9 (720 µg/mL) and to 24.30% ± 4.7 (1000 µg/mL) vs. control (100%). E1, E2 and E4 significantly decreased cell viability starting with 360 µg/mL: 72.18% ± 10.1, 65.70% ± 12.2 and 73.08% ± 8.1 (360 µg/mL), 54.10% ± 14.4, 61.63% ± 10.1 and 61.13% ± 7.7 (720 µg/mL), 34.51% ± 4.3, 53.35% ± 13.2 and 46.84% ± 6.0 (1000 µg/mL) vs. 40.98% ± 2.2 5-FU (100 µM) and vs. control (100%) (Figure 1G–I).

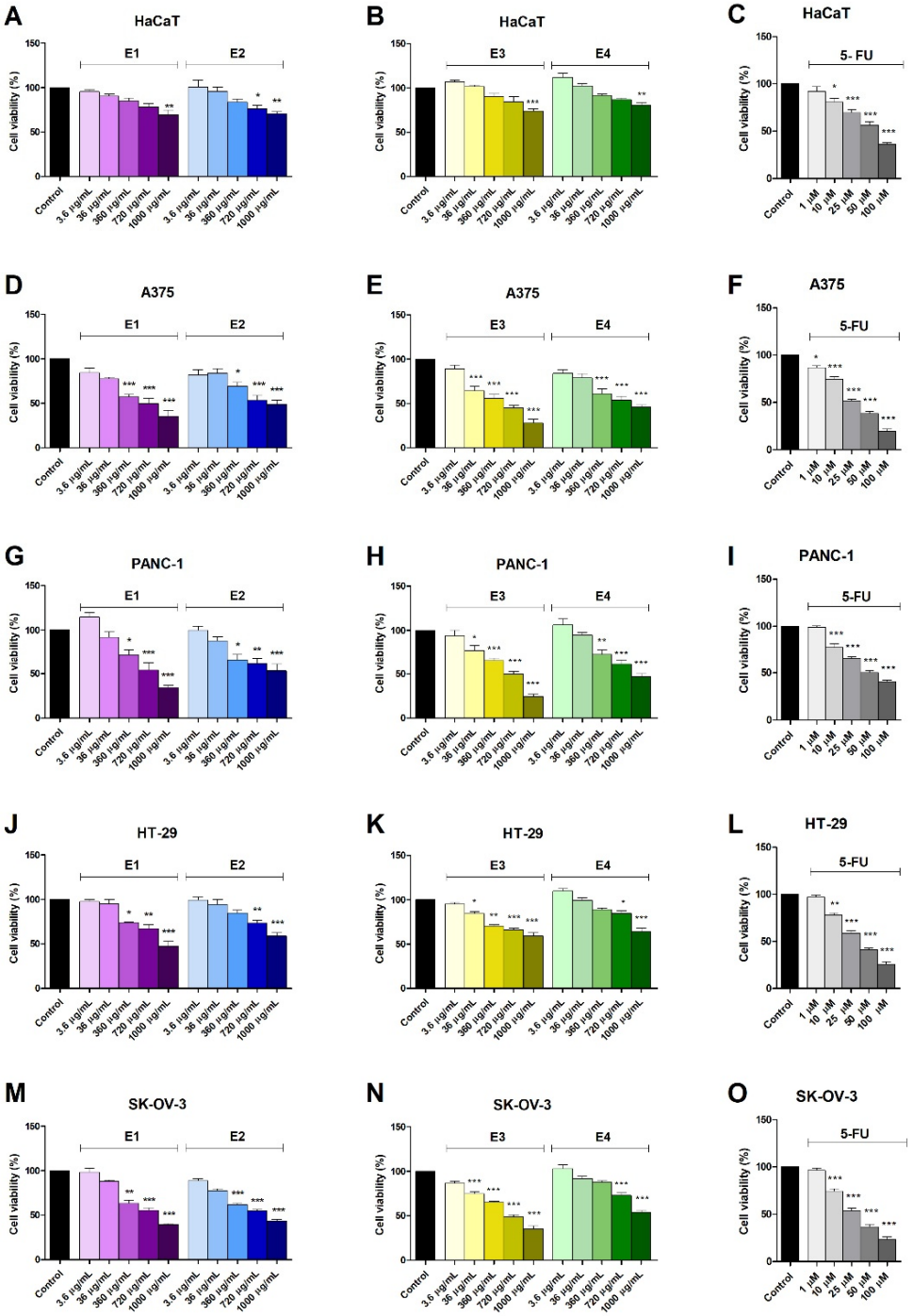

Figure 1. Effects of *E. parviflorum* extracts E1–E4 and 5-FU (positive control) on cell viability. HaCaT (**A**–**C**), A375 (**D**–**F**), PANC-1 (**G**–**I**), HT-29 (**J**–**L**), and SK-OV-3 (**M**–**O**) cells were treated for 24 h with 3.6, 36, 360, 720, and 1000 µg/mL E1–E4 and with 1, 10, 25, 50, and 100 µM 5-FU, respectively. Panels (**A**,**D**,**G**,**J**,**M**) show the effects of E1 and E2; panels (**B**,**E**,**H**,**K**,**N**) show the effects of E3 and E4; and panels (**C**,**F**,**I**,**L**,**O**) show the effects of 5-FU. No macroscopic precipitation was observed in the working solutions at the highest tested concentrations. The results are expressed as viability percentages compared to the control group, considered 100% (* $p < 0.05$; ** $p < 0.01$; *** $p < 0.001$ vs. control cells). The data represents the mean values ± SD of three independent experiments performed in triplicate.

Similar results were observed when all extracts were tested on HT-29 cell line, however, the response observed is more moderate compared to those observed in A375, PANC-1 and SK-OV-3 cell lines. The most notable decrease was observed at 1000 µg/mL for all extracts

(E1–4: 47.65% ± 9.3, 59.23% ± 6.1, 59.41% ± 5.9 and 64.02% ± 6.7), followed by 720 µg/mL (E1–4 67.23% ± 6.1, 73.48% ± 5.3, 66.13% ± 3.0 and 84.66% ± 4.7) and at 360 µg/mL only for E1 (74.09% ± 1.9) and E3 (73.37% ± 3.4) vs. 25.96% ± 4.5 5-FU (100 µM) and vs. control (100%)—Figure 1J–L.

Compared with normal HaCaT cells and with HT-29 cancer cell line, the ovarian SK-OV-3 cancer cell line was more sensitive, especially at intermediate and high concentrations. From all the tested extracts, E3 elicited the most notable decrease in cell viability, as follows: 74.86% ± 3.8 (36 µg/mL), 65.01% ± 2.5 (360 µg/mL), 48.86% ± 4.1 (720 µg/mL) and 35.72% ± 5.2 (1000 µg/mL). Similar decreases were also recorded for E1 and E2 starting with 360 µg/mL: 63.61% ± 5.5 and 61.58% ± 3.0 (360 µg/mL), 55.42% ± 4.9 and 56.96% ± 5.2 (720 µg/mL), 39.36% ± 2.5 and 43.57% ± 3.6 (1000 µg/mL). In contrast, E4 significantly decreased cell viability only at 720 µg/mL (73.16% ± 5.0) and 1000 µg/mL (54.04% ± 4.1) vs. 23.48% ± 5.0 5-FU (100 µM) and vs. control (100%)—Figure 1M–O.

Overall, HaCaT cells appear to be less sensitive to the extracts compared to cancer cell lines, especially at low and intermediate concentrations. However, considering the obtained results and the calculated IC_{50} values, the most relevant candidates for further investigation are those that are able to elicit the highest decrease in the viability of multiple cancer cell lines at doses that preserve HaCaT viability, particularly E1 and E3 (Table 6).

Table 6. The calculated IC_{50} values (µg/mL) of *E. parviflorum* extracts E1–E4 in HaCaT, A375, PANC-1, HT-29 and SK-OV-3 cells after 24 h exposure.

Cell Line	E1	E2	E3	E4	5-FU
HaCaT	>1000	>1000	>1000	>1000	59.92 ± 4.9
A375	664.1 ± 50.7	908.2 ± 61.1	557.4 ± 38.5	832.9 ± 56.5	13.17 ± 1.2
PANC-1	759.5 ± 46.2	993.2 ± 52.1	627.4 ± 25.8	906.69 ± 51.2	63.68 ± 3.7
HT-29	983.8 ± 48.7	>1000	>1000	>1000	34.92 ± 2.9
SK-OV-3	767.1 ± 25.2	808.7 ± 30.7	692.2 ± 31.9	>1000	29.89 ± 1.9

Values >1000 indicate that the IC_{50} was not reached within the tested concentration range.

3.3. Epilobium parviflorum Effect on Cell Morphology

Treatment with 360 µg/mL E1 and E3 induced evident morphological changes in the A375 cells' nuclei and cytoskeleton. In particular, besides cytoskeletal disorganization, loss of structural integrity and the presence of cellular debris/apoptotic body-like structures, the cells' nuclei become more condensed and fragmented after the treatment. All the observed morphological changes are characteristic for non-lytic/apoptotic cell death, especially when compared with the morphological changes induced by staurosporine, the positive control for lytic cell death (Figure 2).

Similar findings were also observed after E1 and E3 treatment in PANC-1 cell line (Figure 3) and SK-OV-3 cell line (Figure 4).

3.4. Epilobium parviflorum Effect on Mitochondrial Respiration

High-resolution respirometry revealed that at 360 µg/mL both E1 and E3 impair mitochondrial respiration in all three tested cancer cell lines (Figures 5–7). This inhibitory effect was noticeable not only in OXPHOS-linked respiration but also in the uncoupled ETS capacity, thus highlighting the global reduction in mitochondrial performance, rather than a selective inhibition of a single respiratory state. Overall, E3 induced the strongest inhibition compared to E1. In the A375 cell line, E1 and E3 significantly decreased all mitochondrial respiratory rates. Across OXPHOS- and ETS-linked states, the values decreased from 47.82 ± 8.5 (OXPHOSCI), 74.28 ± 7.1 (OXPHOSCI+II), 66.63 ± 8.6 (ETSCI+II) and

30.25 ± 5.8 (ETSCII) to 34.02 ± 4.5, 52.34 ± 7.5, 30.53 ± 4.1 and 15.75 ± 3.1 (E1) and to 15.27 ± 5.1, 23.96 ± 4.3, 19.51 ± 3.5 and 11.16 ± 2.8 (E3), respectively (Figure 5).

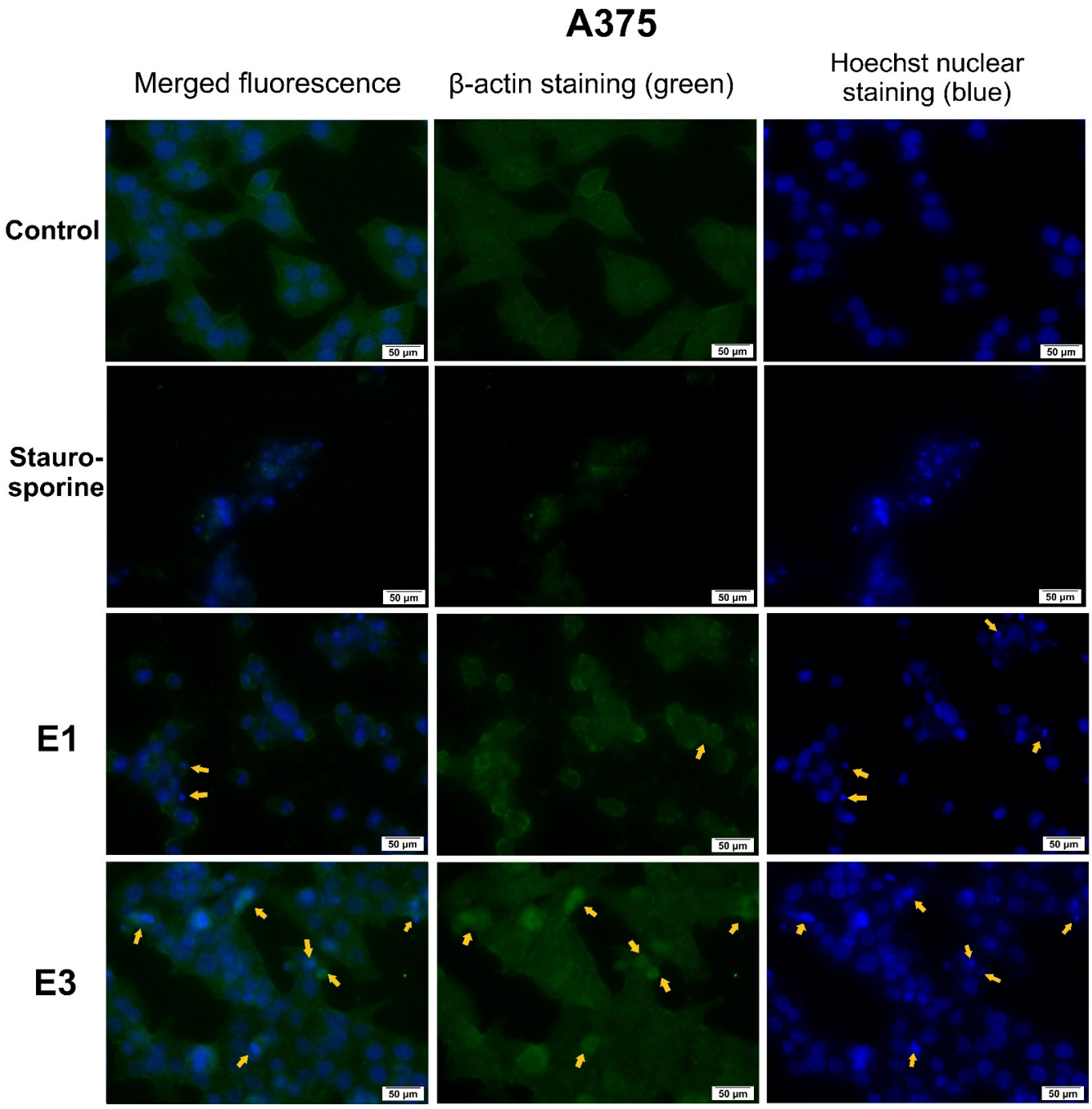

Figure 2. The impact of 24 h treatment with 360 µg/mL E1 and E3 on A375 cells' nuclei (blue—Hoechst staining) and cytoskeleton (β-actin—green staining). Staurosporine (5 µM) was used as a positive control for apoptosis induction. The yellow arrows indicate morphological changes that are suggestive of apoptosis. The scale bar represents 50 µm at 40× magnification.

A similar trend was observed also in PANC-1 cell line; E1 decreased OXPHOSCI and OXPHOSCI+II from 26.33 ± 10.9 and 39.26 ± 3.5 to 19.09 ± 2.7 and 33.85 ± 3.1, respectively, whereas E3 was able to decrease both OXPHOSCI and OXPHOSCI+II to 13.11 ± 1.8 and 24.13 ± 3.4, respectively. ETSCI+II decreased from 55.92 ± 9.9 to 35.62 ± 6.3 (E1) and 30.74 ± 3.3 (E3), while ETSCII decreased from 24.19 ± 4.4 to 12.68 ± 4.0 (E1) and 6.8 ± 2.3 (E3) (Figure 6).

In SK-OV-3 cell line, E1 and E3 reduced OXPHOSCI, OXPHOSCI+II, ETSCI+CII, and ETSCII respiration, with values decreasing from 22.68 ± 5.1, 32.53 ± 4.0, 38.68 ± 4.3 and 28.02 ± 3.2 to 13.67 ± 4.1, 24.08 ± 4.6, 27.03 ± 3.5 and 18.69 ±4.47 (E1) and to 11.35 ± 3.2, 16.09 ± 4.4, 18.14 ± 6.2 and 12.78 ± 3.1 (E3), respectively (Figure 7).

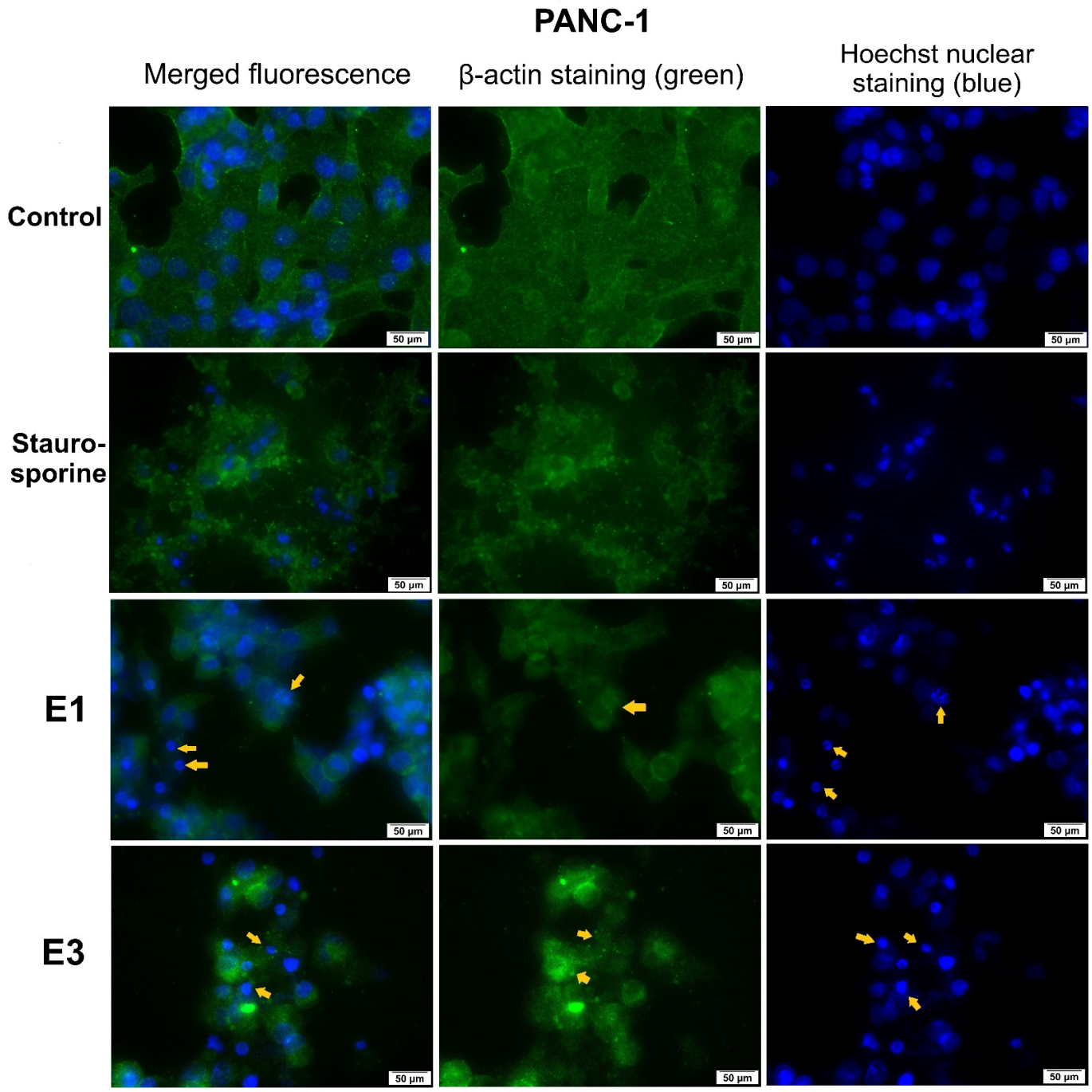

Figure 3. The impact of 24 h treatment with 360 µg/mL E1 and E3 on PANC-1 cells' nuclei (blue—Hoechst staining) and cytoskeleton (β-actin—green staining). Staurosporine (5 µM) was used as a positive control for apoptosis induction. The yellow arrows indicate morphological changes that are suggestive of apoptosis. The scale bar represents 50 µm at 40× magnification.

3.5. Target Prediction and Network Pharmacology

The intersection of potential protein targets for the selected compounds with proteins encoded by relevant melanoma genes yielded 11 shared targets. Among the selected compounds, ellagic acid exhibited the highest target overlap with melanoma-relevant proteins

with nine shared targets (ERBB2, BAP1, HDAC6, IGF1R, CYLD, CTNNB1, HSP90AA1, RAC1, and PTPN13), followed by quercetin with two shared targets (ERBB4 and ZEB2) (Figure 8A). Neither caftaric acid, myricetin nor gallic acid yielded any shared targets under the applied criteria and were further excluded from the analysis. Furthermore, following the STRING network analysis at a high-confidence threshold (>0.7) (Figure 8B), three targets (BAP1, PTPN13 and ZEB2), appeared as disconnected nodes and were excluded, resulting in a final set of eight connected protein targets, namely ERBB2, HDAC6, IGF1R, CYLD, CTNNB1, HSP90AA1, RAC1 and ERBB4 (Figure 8B).

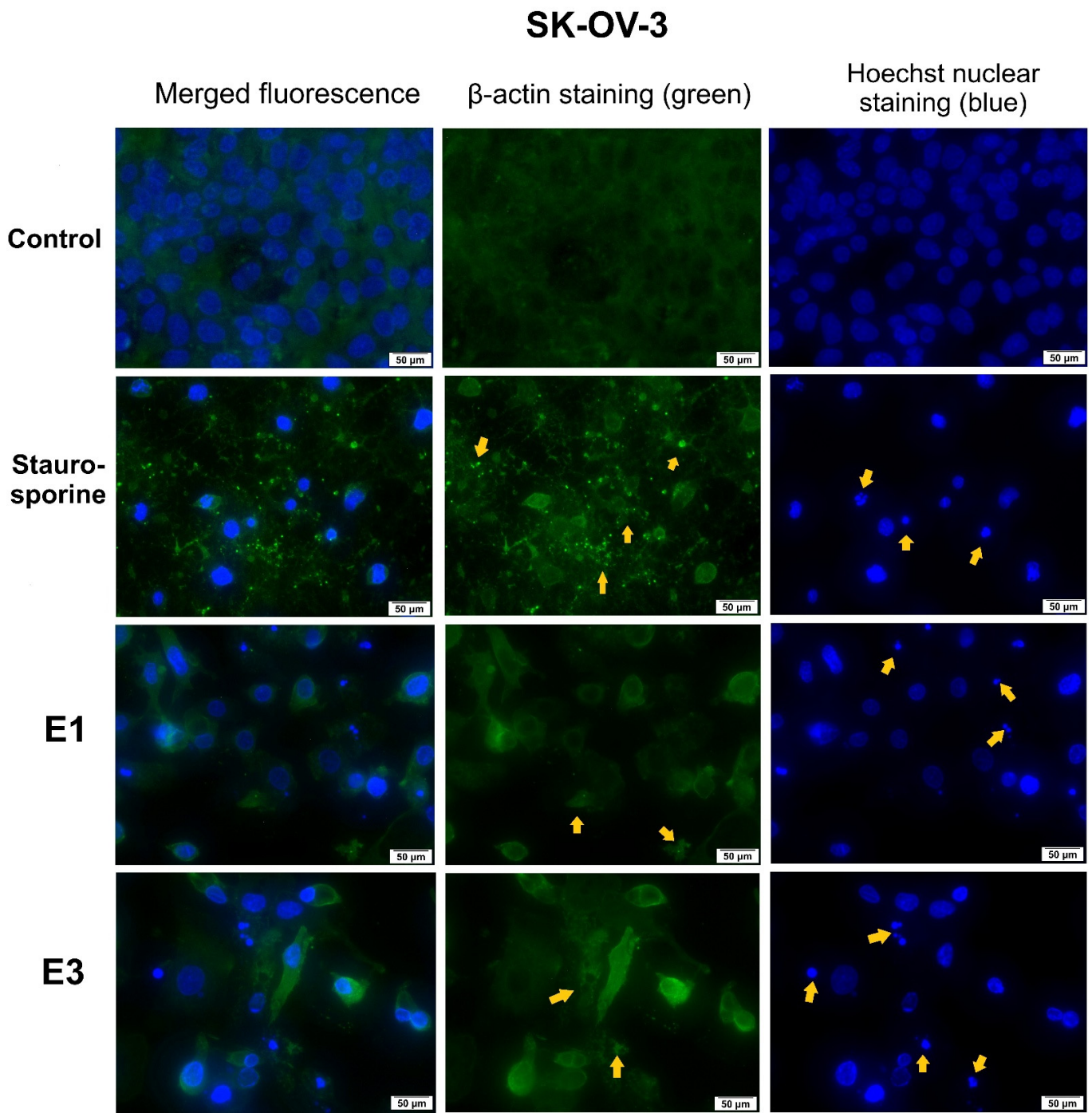

Figure 4. The impact of 24 h treatment with 360 µg/mL E1 and E3 on SK-OV-3 cells' nuclei (blue—Hoechst staining) and cytoskeleton (β-actin—green staining). Staurosporine (5 µM) was used as a positive control for apoptosis induction. The yellow arrows indicate morphological changes that are suggestive of apoptosis. The scale bar represents 50 µm at 40× magnification.

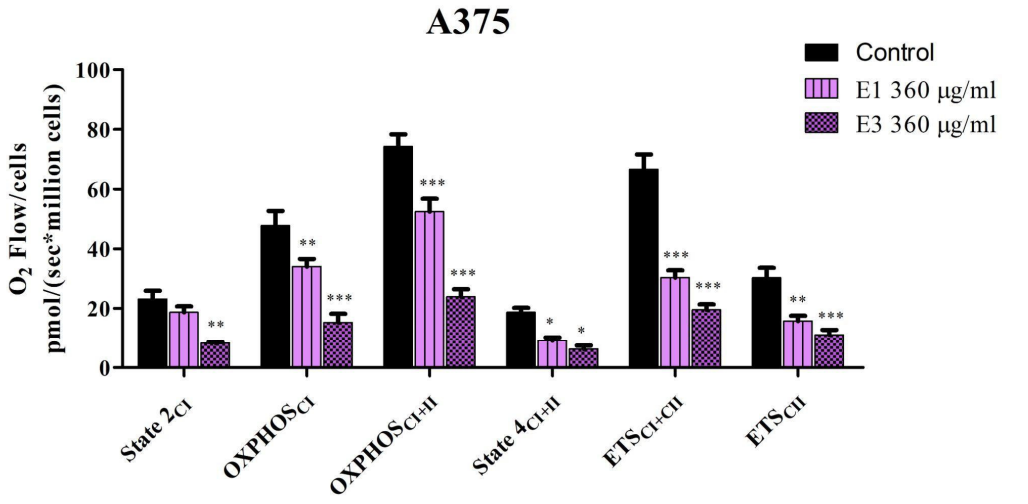

Figure 5. Mitochondrial respiratory rates of permeabilized A375 cells after treatment with 360 µg/mL for E1 and E3. Results are expressed as mean values ± SD of three independent experiments. (* $p < 0.05$; ** $p < 0.01$; *** $p < 0.001$ vs. control cells).

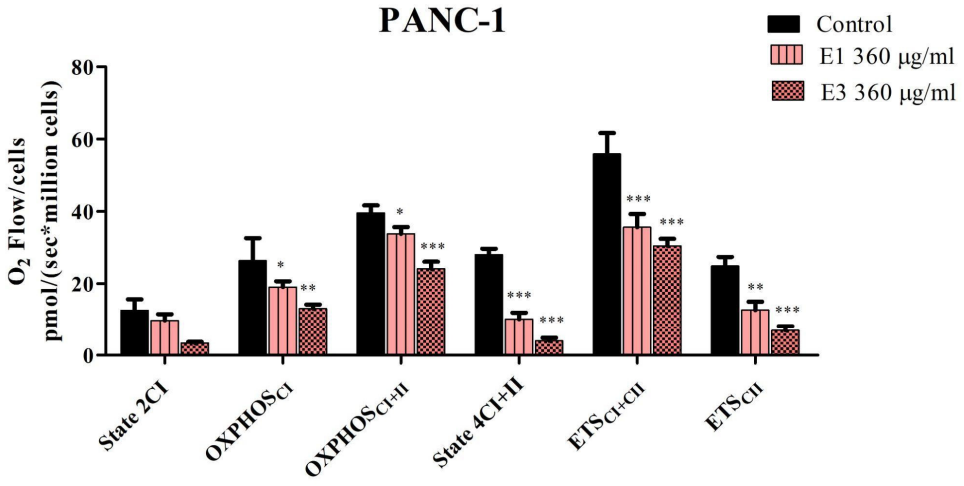

Figure 6. Mitochondrial respiratory rates of permeabilized PANC-1 cells after treatment with 360 µg/mL for E1 and E3. Results are expressed as mean values ± SD of three independent experiments. (* $p < 0.05$; ** $p < 0.01$; *** $p < 0.001$ vs. control cells).

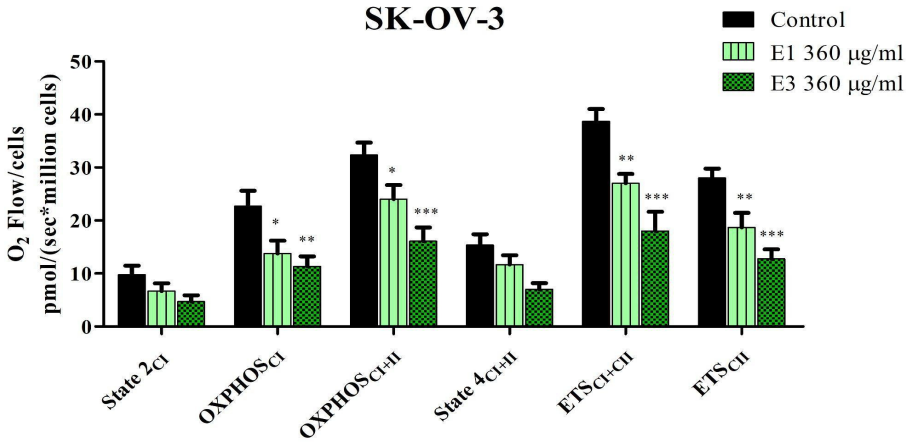

Figure 7. Mitochondrial respiratory rates of permeabilized SK-OV-3 cells after treatment with 360 µg/mL for E1 and E3. Results are expressed as mean values ± SD of three independent experiments. (* $p < 0.05$; ** $p < 0.01$; *** $p < 0.001$ vs. control cells).

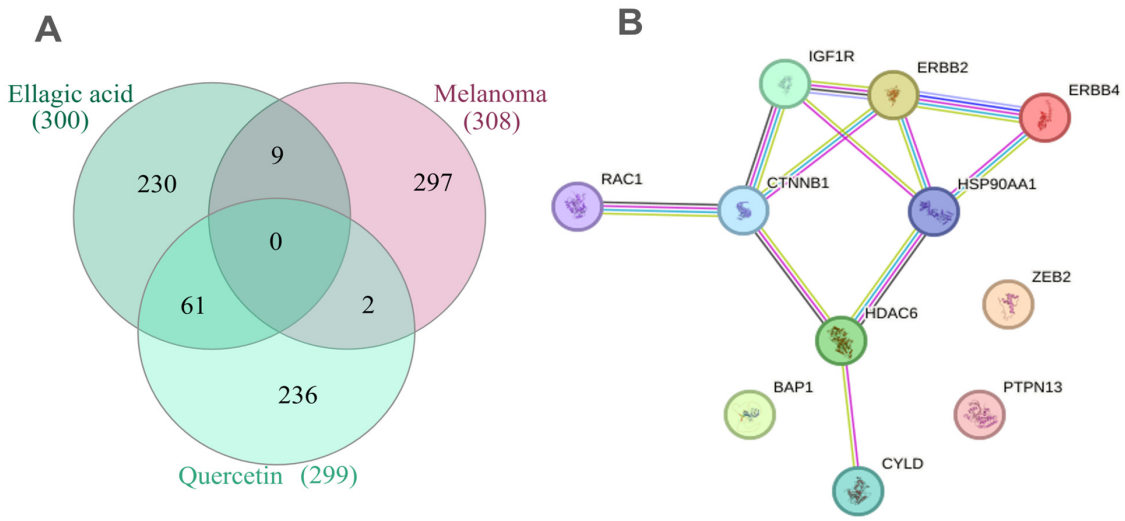

Figure 8. Venn diagram illustrating the overlap between the predicted protein targets of ellagic acid and quercetin with the top melanoma-associated proteins retrieved from GeneCards (Panel (**A**)); STRING protein–protein interaction network of the 11 shared targets at a high-confidence interaction threshold (>0.7) (Panel (**B**)).

The protein–protein interaction network constructed in Cytoscape included eight nodes, represented by the previously connected protein target identified, and 22 edges, representing the interactions between the targets, with a clustering coefficient of 0.33 and a network density of 0.393 (Figure 9A). The topological analysis highlights four potential top targets for ellagic acid and quercetin based on the degree, betweenness centrality and closeness centrality scores, namely ERBB2, CTNNB1, HSP90AA1 and HDAC6 (Table 7).

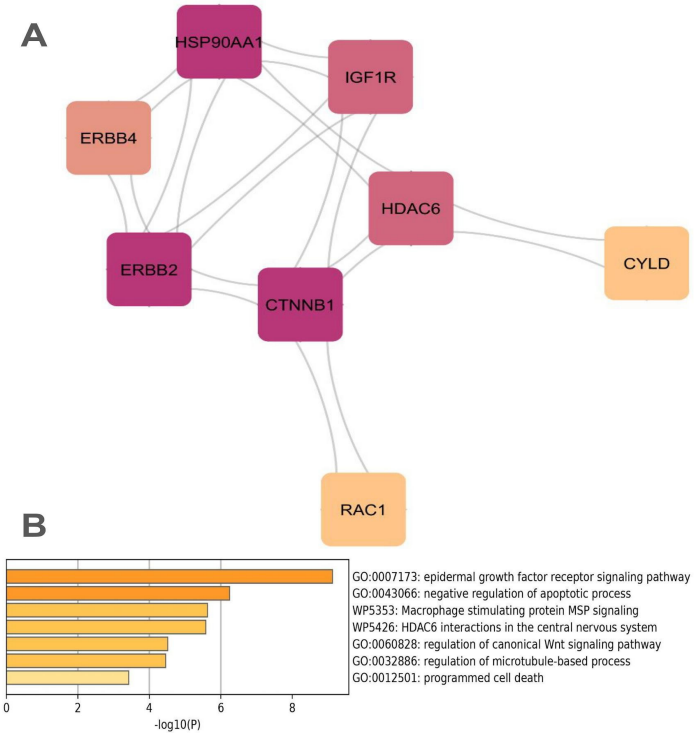

Figure 9. Protein–protein interaction network using yfiles circular layout. The gradient color of the nodes, from beige to dark purple, is proportional to the degree score of the node (Panel (**A**)); functional enrichment analysis highlighting the top biological pathways and processes from KEGG Pathway, GO Biological Processes, and WikiPathways databases. Enrichment significance is expressed as $-\log_{10}(p)$, with longer bars indicating greater statistical significance (Panel (**B**)).

Table 7. Topological parameters of the protein–protein interaction network.

Target	Degree	Betweenness Centrality	Closeness Centrality
ERBB2	8	0.151	0.636
CTNNB1	8	0.7	0.381
HSP90AA1	8	0.214	0.636
HDAC6	6	0.317	0.636
IGF1R	6	0.032	0.583
ERRB4	4	0	0.5
CYLD	2	0	0.412
RAC1	2	0.438	0

The enrichment analysis performed using relevant biological databases (KEGG Pathway, GO Biological Process, and WikiPathways) revealed that the eight targets are predominantly enriched cancer-related pathways and processes (Figure 9B).

3.6. Molecular Docking

Molecular docking was performed to examine the interaction profiles of quercetin and ellagic acid with the four top-ranked targets identified by network topological analysis, namely ERBB2, CTNNB1, HSP90AA1, and HDAC6 (Table 8). Among the investigated targets, the lowest binding energies for both phytocompounds were obtained with ERBB2 and HSP90AA1. In the ERBB2 complex, ellagic acid yielded a binding energy of −9.6 kcal/mol, closely followed by quercetin at −9.4 kcal/mol, whereas the co-crystallized ligand 03Q showed a value of −11.1 kcal/mol. Therefore, although both phytocompounds were accommodated within the selected ERBB2 binding site, their predicted affinities remained lower than that of the reference ligand. For HSP90AA1, ellagic acid and quercetin yielded binding energies of −9.3 and −9.0 kcal/mol, respectively, compared with −8.6 kcal/mol for the co-crystallized ligand EOR. In this case, both phytocompounds displayed slightly lower calculated binding energies than the reference ligand, with ellagic acid showing the lowest value among the three compounds.

Table 8. Molecular docking results of quercetin and ellagic acid against the selected protein targets.

Co-Crystallized Ligand	Native Ligand Docking Score (kcal/mol)	Quercetin (kcal/mol)	Ellagic Acid (kcal/mol)
03Q	−11.1	−9.4	−9.6
R9Q	−6.2	−5.8	−6.2
EOR	−8.6	−9.0	−9.3
TSN	−8.4	−7.1	−6.8

In contrast, less favorable docking scores were obtained for CTNNB1 and HDAC6, particularly for quercetin against CTNNB1 and for both phytocompounds against HDAC6 when compared with the corresponding co-crystallized ligands.

The three-dimensional binding poses of ellagic acid and quercetin within the HSP90AA1 binding site are shown in Figure 10. Ellagic acid (Figure 10A) adopted a relatively compact orientation within the binding cavity, with its fused aromatic scaffold positioned predominantly within hydrophobic regions of the pocket, while its oxygen-containing groups were oriented toward less hydrophobic areas. Quercetin (Figure 10B) displayed a more extended binding orientation, spanning a broader region of the cavity. Its aromatic rings were accommodated within hydrophobic regions, whereas the hydroxyl and carbonyl groups were preferentially oriented toward more polar areas of the binding site. These differences in spatial accommodation were accompanied by slightly different

docking scores, with ellagic acid showing a binding energy of −9.3 kcal/mol compared with −9.0 kcal/mol for quercetin.

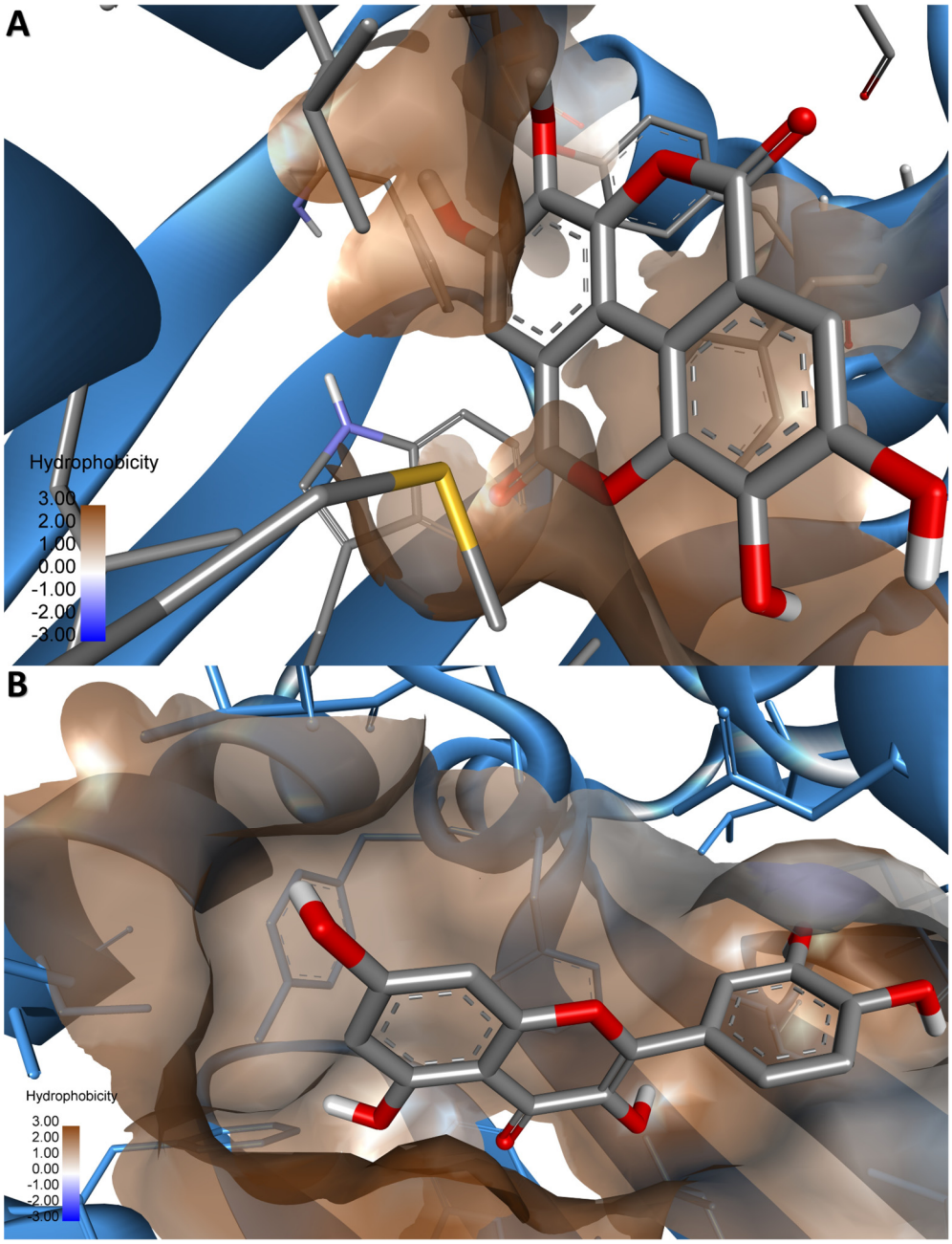

Figure 10. Three-dimensional representation of the predicted binding poses of ellagic acid (**A**) and quercetin (**B**) within the HSP90AA1 binding site (PDB ID: 6LR9). The binding-site surface is represented according to hydrophobicity, ranging from hydrophilic (blue) to hydrophobic (brown) regions.

The analysis of the surrounding amino acid environment further showed that the two ligands occupied largely overlapping regions of the HSP90AA1 binding pocket (Figure 11A,B). Several residues were located in the vicinity of both compounds, including Leu29, Met30, Ile33, Ile91, Phe138, Tyr139, Ala141, Ala145, Val148, Val186, and Leu188. Despite this common binding environment, the two ligands adopted distinct orientations within the cavity, reflecting differences in their molecular geometry and distribution of oxygen-containing functional groups. The extensive positioning of their aromatic scaffolds within the surrounding non-polar environment is consistent with the hydrophobic complementarity observed in the surface representations (Figure 10A,B).

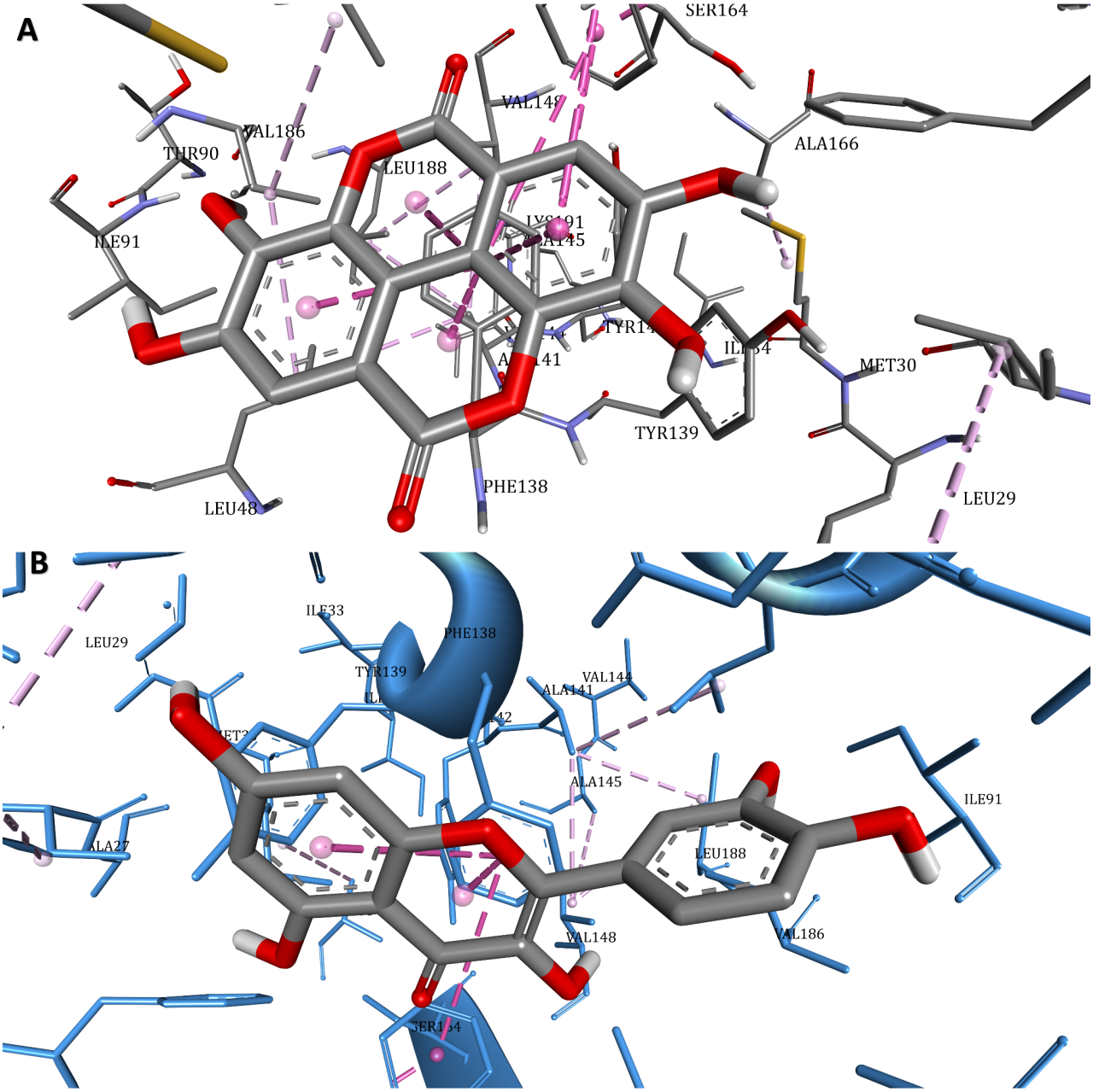

Figure 11. Three-dimensional representation of the predicted binding modes of ellagic acid (**A**) and quercetin (**B**) within the HSP90AA1 binding site (PDB ID: 6LR9), showing the surrounding amino acid residues.

The two-dimensional interaction analysis further revealed distinct interaction patterns for the two compounds (Figure 12). Ellagic acid formed a conventional hydrogen bond with Tyr139, while its aromatic scaffold was involved in several π-mediated contacts, including interactions with Leu107 and Phe138, together with a π–sulfur interaction involving Met98. Additional van der Waals contacts contributed to its accommodation within the binding site. Quercetin displayed a more extensive hydrogen-bonding pattern, involving Tyr139, Gly135, and Asp93, accompanied by π-mediated interactions with Phe138, Leu107, and Ala111 and several surrounding van der Waals contacts. Notably, Tyr139, Phe138, and Leu107 were involved in the interaction profiles of both ligands, indicating partially shared molecular recognition within the HSP90AA1 binding pocket. Despite the larger number of hydrogen bonds observed for quercetin, ellagic acid showed a slightly lower docking energy (Table 8),

suggesting that the calculated binding score reflects the combined contribution of multiple non-covalent interactions rather than hydrogen bonding alone.

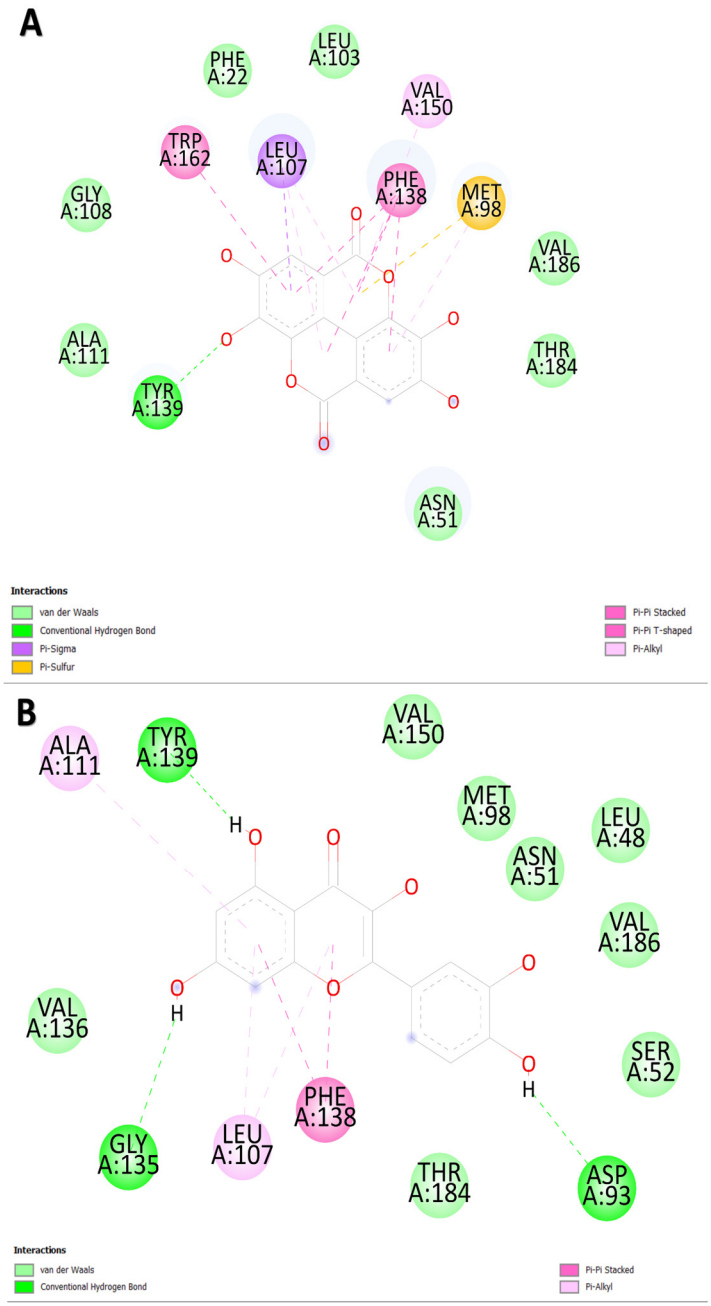

Figure 12. Two-dimensional interaction diagrams of ellagic acid (**A**) and quercetin (**B**) within the predicted HSP90AA1 binding site (PDB ID: 6LR9), showing hydrogen bonds, van der Waals contacts, and π-mediated interactions identified using BIOVIA Discovery Studio Visualizer 2024.

4. Discussion

The current study provides preliminary significant evidence regarding the phytochemical composition and cytotoxic potential of hydroalcoholic extracts prepared from the aerial parts of *E. parviflorum* Schreb. The comparative assessment of the four extracts obtained through various extraction procedures using different solvents allowed the identification of chemical differences due to extraction and also differences in the biological effects exerted against several cell lines.

The phytochemical assessment of the four *E. parviflorum* extracts revealed that the extraction parameters influenced the recovery of different phenolic compounds. E2 and E4 extracts displayed the highest TPC and TFC values which suggests that the 60% ethanol composition favored the extraction of phenols and flavonoids, presumably due to the fact that hydroalcoholic solvents combine the water-mediated swelling of the plant matrix with ethanol's ability to solubilize compounds of moderate polarity. Consequently, the 60% ethanol:water solvent produced extracts richer in total phenolic and flavonoid compounds compared to the 40% ethanol:water counterpart. The similar profile reported for TPC and TFC suggests that flavonoids contributed in part to the Folin–Ciocalteu reaction which is consistent with the already reported phytochemical composition of *Epilobium* species consisting of flavonoids such as quercetin, myricetin, kaempferol and their glycosides, together with phenolic acids and tannins [6,37]. However, since the Folin–Ciocalteu assay is not specific for phenolic compounds alone but rather assesses the overall reducing capacity of the sample, the TPC values should be regarded as gallic acid equivalent Folin-reactive components rather than individual polyphenols [38].

In contrast to TPC and TFC, the condensed tannin content followed a different pattern. E3 and E4 extracts revealed the highest CTC values, while E2, although showing the highest TPC and TFC values, displayed the lowest CTC thus suggesting that condensed tannins represented only a limited fraction of the total phenolic content of the investigated extracts. The CTC values, ranging from 8.73 $\pm$ 0.05 to 11.71 $\pm$ 0.09 mg CE/g extract, confirm the presence of condensed tannins in the analyzed extracts but also indicate that such compounds are not the main contributors to the total phenolic content. These findings are in agreement with previous studies that reported the occurrence of condensed tannins in *E. parviflorum* extracts based on their reaction with vanillin; as an example, Merighi et al. reported condensed tannin contents of 1.04 $\pm$ 0.01, 1.43 $\pm$ 0.01 and 0.56 $\pm$ 0.06 µg CE/µL liquid extract for hot glycerate, cold glycerate and 40% ethanolic *E. parviflorum* extracts, respectively [39]. Conversely, compared to the current study, Kyriakou et al. reported different condensed tannin values for *E. parviflorum* dry extracts [6], presumably due to variations in plant origin, extraction procedure, fraction type and standardization approach. Moreover, the vanillin assay can be influenced by several experimental parameters, such as the solvent composition, reaction time, temperature, pH as well as the molecular structures of the tannins [40]. Therefore, CTC values obtained as a result of this colorimetric method should be interpreted as catechin-equivalent estimates rather than as absolute concentrations of all condensed tannins. Consequently, liquid chromatography remains essential to identify individual flavonoids, phenols and tannins.

The LC-MS analysis performed in negative ion SIM mode revealed the presence of flavonols in the *E. parviflorum* extracts, with hyperoside as the main compound; hyperoside was identified in all four samples in comparable amounts, ranging from 24.28 to 26.49 µg/mg d.e., which indicates the limited influence exerted on its recovery by both the extraction technique and the ethanol concentration. The predominance of hyperoside is consistent with previous phytochemical investigations on *Epilobium* species. Karakaya et al. reported hyperoside as a major compound in several *Epilobium* species and highlighted its significance for the quality control and biological activity assessment of their extracts [41]. Similarly, Vlase et al. indicated hyperoside, isoquercitrin, quercitrin, rutin, myricetin, quercetin, kaempferol, luteolin and related phenolic acids as analytical standards used for the LC-MS/MS characterization of Romanian *Epilobium* species thus confirming their significance in the phytochemical analysis of this genus [42]. Although hyperoside is the main compound, the content in other flavonoids varied according to the extraction procedure; as such, myricetin is the second most abundant compound in the E1 extract, reaching much lower concentration in E2 and being below the quantification limit in both

Soxhlet extracts presumably due to the prolonged exposure to high temperature since the hydroxylated flavonols are generally significantly prone to oxidative and thermal degradation. Consequently, maceration with hydroalcoholic solvents appears to better preserve or extract thermolabile phenolic components. Similar findings were reported by Vlase et al. who pinpointed the relevance of solvent composition for the preparation of extracts with optimal phytochemical and biological properties [42]. Isoquercitrin was detected in much lower amounts compared to hyperoside in all four extracts; since the two compounds are structural isomers, the higher level of hyperoside may be attributed to the predominance of the galactosylated quercetin derivative over its glucosylated analog. Phenolic acids were present merely in minor amounts compared to the flavonol glycosides; among them, caftaric acid was the most abundant, with concentrations ranging between 2.38 and 2.97 μg/mg d.e., while other acids (i.e., gentisic, chlorogenic, caffeic, ferulic, sinapic and p-coumaric acid) occurred in much lower amounts or were below the quantification limit. Such low levels of phenolic acids may be related to the origin of the vegetal material, harvest conditions, drying and extraction parameters or the limitations of the SIM method. The minor flavonoid content is also influenced by the extraction procedure; as such, the 40% ethanol maceration favored the recovery of minor flavonoids. However, Mohammadi Bazargani et al. emphasized the relevance of environmental factors, plant organ and phenological stage in the composition of *E. hirsutum* and *E. parviflorum* populations [43]. Consequently, the reported differences should be regarded in relation to the extraction parameters but also considering the natural phytochemical variability of the plant material. An important limitation of the current LC-MS analysis is that the SIM method involved the use of a predefined panel of 18 phenolic components, therefore failing to provide a complete characterization of the *E. parviflorum* phytocomposition. This is particularly relevant since there are studies reporting that *Epilobium* species are also rich in hydrolysable tannins, mainly oenothein B, which is frequently indicated as their major bioactive components [7,42]. Consequently, the current data indicate hyperoside as the major compound among those tested but not necessarily of the entire extract. In terms of pharmacological assessment, the high amount of hyperoside may be responsible for the antioxidant and anti-inflammatory properties of *Epilobium* extracts [7,39] reported in recent studies, although these activities are more probably the result of synergistic interactions among various classes of phytocompounds instead of a single compound. Therefore, its presence in the investigated extracts supports its use as an analytical marker for standardization procedures, while the biological activity of the extracts should be assessed in relation to their more complex composition.

The extraction yields were comparable among the four preparations, ranging from 15.58% to 18.22%, with the highest value occurring for E3, followed closely by E1. The fact that both 40% ethanol extracts revealed either the highest extraction yield or the strongest biological effect is consistent with previous reports that indicated hydroalcoholic solvents for the extraction of polar and moderately polar phenolic compounds from *Epilobium* species [39,42]. However, the extraction yield does not fully predict the biological activity, since E3, although displaying lower TPC and TFC compared to E2 and E4, exerted stronger in vitro antiproliferative effects thus indicating that the extraction efficiency should also be interpreted qualitatively, considering that the biological activity is directly related to the relative abundance of bioactive constituents, the presence of other unidentified compounds and also potential synergistic intercomponent interactions.

In terms of the potential relationship between phytochemical composition and observed biological activity, hyperoside, the major compound in all extracts, may be an important contributor, as it has been reported to inhibit cancer-cell proliferation and to induce ROS-mediated apoptosis [44]. Myricetin may also be involved in the antiproliferative and mitochondrial effects through apoptosis induction and PI3K/Akt/mTOR signaling

inhibition [45]. The presence of gentisic acid, caftaric acid and quercitrin could provide complementary effects owing to their described biological and redox-modulating activities [46–48]. In summary, the cytotoxic effects of *E. parviflorum* extracts are probably due to the synergistic effect of different phenolic components rather than a single compound.

The biological evaluation provides preliminary but significant evidence in terms of the in vitro cytotoxic activity of *E. parviflorum* hydroalcoholic extracts against four cancer cell lines of various origins. A375 human melanoma cells are suitable models for the assessment of compounds with potential effects against aggressive skin cancers, particularly since previous studies have already reported the anti-melanoma activity of *E. parviflorum* extracts [6]. HT-29 cells, derived from human colorectal adenocarcinoma, are frequently used as gastrointestinal cancer models and were employed in the assessment of the antiproliferative and pro-apoptotic effects of *E. parviflorum* extracts, including the modulation of caspase-3 and caspase-8 expression [10]. PANC-1 cells are derived from pancreatic carcinoma and frequently serve as in vitro models for the study of potential therapeutics against pancreatic cancer particularly considering its aggressiveness and poor prognosis [14,49]. SK-OV-3 cells, derived from ovarian adenocarcinoma, are widely used as ovarian cancer models for drug response and resistance studies, thus being relevant in the preliminary evaluation of new antiproliferative agents [50].

All tested extracts reduced cancer cell viability in a dose dependent manner, while HaCaT keratinocytes were less affected, particularly when low and intermediate concentrations were used, thus suggesting a certain degree of selectivity toward malignant cells. Extract E3 showed the lowest IC_{50} values in A375 melanoma cells, PANC-1 pancreatic carcinoma cells and SK-OV-3 ovarian adenocarcinoma cells, with IC_{50} values of 557.4 μg/mL, 627.4 μg/mL and 692.2 μg/mL, respectively, followed by E1 which also showed relevant activity. Although the extracts induced a concentration-dependent reduction in cancer cell viability, the most pronounced effects were observed for the highest concentration range tested. Considering their complex and unfractionated nature, further fractionation and evaluation of the enriched fractions and isolated constituents is warranted. In contrast, all extracts displayed IC_{50} values above 1000 μg/mL in HaCaT cells, thus suggesting lower toxicity in non-tumor keratinocytes compared to cancer cells, an important aspect for selective cytotoxic candidates. The sensitivity of A375 melanoma cells to *E. parviflorum* extracts is consistent with previous data that showed that methanolic extracts reduced the viability of A375 and COLO-679 melanoma cells in a time- and concentration-dependent manner, while leaving HaCaT keratinocytes practically unharmed [6]. The present findings add to the existing data by showing that hydroalcoholic extracts, particularly E3, also exert a strong antiproliferative effect against A375 cells. Compared to the other three cell lines, HT-29 colorectal adenocarcinoma cells showed a more moderate response; when used in the highest concentration, all extracts decreased HT-29 viability, but only the E1 extract displayed an IC_{50} value below 1000 μg/mL. This limited response does not contradict previous reports, but rather reveal the significance of the extraction method, solvent composition, exposure time and extract standardization; in this regard, earlier studies reported that aqueous and ethanolic *E. parviflorum* extracts reduced HT-29 cell viability in a dose-dependent manner by inducing apoptotic events [10]. The antiproliferative effects recorded in PANC-1 cells are particularly important due to the poor prognosis, high aggressiveness and limited therapeutic response that characterize pancreatic cancer [14]. E3 extract induced a marked dose-dependent decrease in PANC-1 viability, with an IC_{50} of 627.4 μg/mL, followed by E1 that also showed relevant activity. Since mitochondrial oxidative processes are increasingly recognized as promising therapeutic targets in pancreatic ductal adenocarcinoma, the antiproliferative effect of E1 and E3 combined with their inhibitory effect on mitochondrial respiration indicate their interference with cancer cell

bioenergetics as the underlying molecular mechanisms [51]. The sensitivity of SK-OV-3 ovarian adenocarcinoma cells further expand the cytotoxic range of *E. parviflorum;* SK-OV-3 cells reacted strongly to the application of E1, E2 and E3 extracts with E3 being the most active and reducing cell viability in a dose-dependent manner.

The morphological analyses are in agreement with the cytotoxicity data thus suggesting that the reduction in cell viability may be associated, at least partly, with apoptotic cell death. Treatment with the E1 and E3 extracts induced clear changes in the nuclear morphology and cytoskeletal organization in A375, PANC-1 and SK-OV-3 cells, being typical morphological hallmarks of apoptosis [52]. These findings are in line with previous studies that reported apoptotic effects of *E. parviflorum* extracts in HT-29 cells and of other *Epilobium* species extracts in hormone-dependent prostate cancer cells [9,10].

The high-resolution respirometry provides additional mechanistic information, particularly for A375, PANC-1 and SK-OV-3 cells. The treatment with E1 and E3 extracts was able to reduce several mitochondrial respiratory parameters, such as complex I oxidative phosphorylation, combined complex I and II respiration and electron transfer system capacity dependent on both complex I and II, as well as complex II electron transport capacity. This activity suggests that the extracts are able to alter the mitochondrial oxidative metabolism instead of simply acting as non-specific cytotoxic agents. The decrease in both OXPHOS- and ETS-linked respiration stands as evidence for a potential limitation of the electron transport chain function and mitochondrial energy production. This is particularly relevant since mitochondria act as major regulators of both cancer cell metabolism and intrinsic apoptosis and natural compounds have been frequently investigated for their ability to target mitochondrial function in cancer cells [51,53].

The mitochondrial effects were especially obvious in A375 cells where E3 reduced OXPHOSCI from 47.82 ± 8.5 to 15.27 ± 5.1, OXPHOSCI+II from 74.28 ± 7.1 to 23.96 ± 4.3, ETSCI+II from 66.63 ± 8.6 to 19.51 ± 3.5 and ETSCII from 30.25 ± 5.8 to 11.16 ± 2.8. Similar inhibitory patterns were observed in PANC-1 and SK-OV-3 cells when 360 µg/mL E3 was applied, a lower concentration than the calculated IC_{50} values for E1 and E3 in the respective cancer cell lines, thus suggesting that mitochondrial dysfunction may occur as an early event that contributes to the subsequent decrease in cell viability. Our data are consistent with previous reports on *Epilobium* species. Stolarczyk et al. showed that *Epilobium* extracts induced apoptosis in hormone-dependent prostate cancer cells through the activation of mitochondrial pathways, including loss of mitochondrial membrane potential and caspase-3 activation [9]. In the current study, the combined effects of decreased mitochondrial respiration, reduced cell viability and apoptotic morphological changes support the formulated hypothesis that mitochondrial dysfunction significantly contributes to the cytotoxic effects of *E. parviflorum* extracts.

The selective effects against cancer cells vs. HaCaT keratinocytes may be explained by the well-known differences between cancer and healthy cells in terms of metabolic parameters, mitochondrial function, redox balance and ability to react to stress. Cancer cells are frequently more dependent on metabolic plasticity compared to non-cancer cells and are therefore more susceptible to compounds able to modulate the oxidative phosphorylation, redox homeostasis or mitochondrial integrity. Certain compounds, such as polyphenols may display a dual behavior by acting as antioxidants in non-malignant cells and pro-oxidant or mitochondria-disruptive compounds in cancer cells, depending on their concentration, cellular media and metabolic phenotype [13,53].

Collectively, the current findings are consistent with the previously reported cytotoxic activity of *E. parviflorum* in prostate, colorectal, breast and melanoma cancer cells [6,9–11]. The novelty of the present study resides in the comparative assessment of the four extracts in several tumor cell lines, including PANC-1 and SK-OV-3 cells where data regarding

E. parviflorum are still limited. The results indicate that E3, prepared by means of Soxhlet extraction in 40% ethanol, is the most promising extract for future investigations, followed by E1, obtained by maceration in 40% ethanol.

Network pharmacology is an integrated bioinformatic approach that enables the study in silico of potential molecular targets of plant extracts, which are known for their complex composition [54]. Although many network pharmacology studies include in the network analysis all the components detected in the extract [55], others focus only on selected pharmacologically relevant compounds [56]. In the current study, five representative constituents of *E. parviflorum* aerial parts, namely caftaric acid, ellagic acid, gallic acid, quercetin (quercetol), and myricetin, were selected for a network pharmacology study to identify potential molecular targets responsible for the cytotoxicity observed against the A375 cell line (melanoma), the most sensitive cell line among the panel assessed in vitro. While the HPLC-MS analysis confirmed the presence of caftaric acid, quercetin and myricetin in the hydroalcoholic extracts tested, ellagic acid and gallic acid were included in the analysis, despite not being chromatographically identified due to the absence of the appropriate reference standards in the HPLC protocol employed. They were selected based on previous reports on the composition of similar hydroalcoholic extracts of *Epilobium parviflorum* aerial parts [6,57]. Additionally, hyperoside and isoquercitrin were excluded from the analysis despite being chromatographically identified as significant components of the extracts studied, as both are glycosylated derivatives of quercetin that undergo intestinal hydrolysis in vivo to form quercetin, which is already included in the analysis [58,59].

ERBB2, CTNNB1, HSP90AA1, and HDAC6 emerged as the top targets within the protein–protein interaction network, suggesting their potential relevance for the cytotoxicity observed in the A375 (melanoma) cell line of *E. parviflorum* extract. Nevertheless, further studies are required to validate these predictions and confirm their biological significance. Interestingly, these targets were initially identified through reverse pharmacophore mapping as potential targets only for ellagic acid, indicating that among the compounds included in the network pharmacology analysis, ellagic acid displayed the greatest overlap with melanoma-associated proteins, potentially contributing to the cytotoxicity observed in the A375 cell line. However, because ellagic acid was included in the analysis based on literature reports and its presence in the extracts could not be confirmed due to methodological limitations, the present findings should not be interpreted as evidence that ellagic acid is the primary compound responsible for the cytotoxicity, but rather as a hypothesis worth exploring in the future.

Previous studies of purified ellagic acid and quercetin in the A375 cell line support their cytotoxic potential. Ellagic acid induced apoptosis and inhibited cell proliferation in a dose-dependent manner at concentrations ranging from 5 to 80 μM at 48 h exposure, although the IC_{50} value was not reported [60]. In addition, quercetin induced dose-dependent cytotoxicity in the A375 cell line with an IC_{50} value of 11.08 μM, with no significant effect in the HaCaT cell line [61]. While these findings cannot be directly extrapolated to the cytotoxicity observed for the E. parviflorum extract, they provide support for the network pharmacology analysis. Purified ellagic acid and quercetin also showed cytotoxic potential against HT-29, PANC-1 and SK-OV-3 cell lines. In the HT-29 cell line, ellagic acid extracted from an ayurvedic formulation induced apoptosis, cell cycle arrest and cytotoxicity (IC_{50}: 13.1 μg/mL) [62], while quercetin exerted a dose-dependent cytotoxicity with an IC_{50} value of 160.63 μM. In the PANC-1 cell line, both ellagic acid and quercetin exerted time and dose-dependent cytotoxicity with IC_{50} values ranging from 7.38 μg/mL (24 h) to 5.41 μg/mL (48 h) for ellagic acid [63] and from 12.14 μmol/L (24 h) to 4.578 μmol/L (48 h) for quercetin [64]. Lastly, in SK-OV-3 cell line, previous studies show ellagic acid and

quercetin induced cytotoxicity with IC_{50} value of 36.6 μmol/L [65] and 16.21 μg/mL [66], showing that both compounds have the ability to induce cytotoxicity in selected cell lines.

The enrichment analysis highlighted the role of the identified targets into the epidermal growth factor receptor signaling pathway (GO:0007173) (Figure 9, Panel B), whose activation in melanoma is associated with enhanced proliferation and aggressiveness [67,68]. These findings are consistent with a previous study reporting decreased proliferation of A375 and WM115 melanoma cell lines exerted by ellagic acid through the inhibition of the EGFR signaling pathway [69]. Negative regulation of the apoptotic process, programmed cell death and Wnt signaling pathways were also enriched (Figure 9, Panel B), suggesting that ellagic acid and quercetin might be responsible for the apoptosis exerted in the A375 cell line by the *E. parviflorum* extract. These findings are consistent with previous studies on individually studied quercetin and ellagic acid, which indicate the induction of apoptosis in melanoma cell lines [58,61]. Nevertheless, the predictive nature of the network pharmacology analysis employed should be acknowledged as a limitation that needs further validation through biological assays.

Molecular docking was used to investigate the binding of ellagic acid and quercetin to the four targets identified by network pharmacology. Both compounds showed the most favorable predicted binding toward ERBB2 and HSP90AA1, whereas less favorable docking scores were obtained for HDAC6 and CTNNB1. The interaction with HSP90AA1 was particularly notable, as ellagic acid and quercetin yielded slightly lower docking energies than the co-crystallized ligand EOR. Both compounds were accommodated within the HSP90AA1 binding pocket, although differences were observed in their orientations and interaction patterns. Despite the more extensive hydrogen-bonding pattern observed for quercetin, ellagic acid showed a slightly lower docking energy, indicating that the predicted binding may result from the combined contribution of different non-covalent interactions within the binding site. These docking results are consistent with the network pharmacology findings, particularly regarding HSP90AA1. Nevertheless, molecular docking remains a predictive approach, and the predicted interactions of these compounds with the proposed targets require experimental validation.

Several limitations should be acknowledged in the current study. First, since the extracts are highly complex mixtures, certain active constituents may still remain to be identified and quantified. Therefore, a more thorough HPLC/MS analysis can be essential to enable a direct correlation between the chemical composition and the biological activity. Second, the current viability results were obtained following a 24 h exposure, by means of a metabolic assay; therefore, additional assays would strengthen their interpretation. Third, specific biochemical assays such as caspase-3/7 activation, Bax/Bcl-2 ratio, cytochrome c release, mitochondrial membrane potential, ROS production and ATP levels should be performed in the future in order to confirm apoptosis and mitochondrial involvement. Finally, future studies should include the use of standardized extracts, isolated major compounds, such as hyperoside, longer exposure times and validation in more complex models, such as 3D tumor spheroids.

5. Conclusions

The current study provides preliminary data regarding the in vitro cytotoxic activity of *E. parviflorum* hydroalcoholic extracts against several human cancer cell lines; all four extracts induced a dose-dependent decrease in cancer cells' viability following 24 h exposure. Among the tested extracts, the Soxhlet extraction using 40% ethanol triggered the strongest antiproliferative effect, particularly in A375, PANC-1 and SK-OV-3 cells. Maceration in 40% ethanol also led to a significantly active extract which was also the only one characterized by an IC_{50} value below 1000 μg/mL in HT-29 cells. In contrast, all extracts revealed IC_{50}

values above 1000 μg/mL in HaCaT normal keratinocytes thus suggesting a certain degree of selectivity against malignant cells.

The morphological assessments further supported the antiproliferative findings, with E1 and E3 inducing nuclear condensation and fragmentation, cytoskeletal ruptures and the occurrence of apoptotic elements in cancer cells, changes that indicate apoptotic cell death and add to the nonspecific cytotoxicity.

E1 and E3 extracts also alter the mitochondrial respiratory function by reducing the oxidative phosphorylation and the electron transport system capacity, therefore suggesting that the mitochondrial dysfunction may represent one of the mechanisms involved in their cytotoxic activity.

The phytochemical analysis identified 15 polyphenols, with hyperoside as the predominant compound, followed by caftaric acid, gentisic acid, myricetin and quercitrin. However, due to the complex composition of these extracts, the observed antiproliferative, morphological and mitochondrial effects cannot be attributed to a single constituent.

Additionally, the network pharmacology analysis indicated that the cytotoxic activity recorded in melanoma cells may be mediated through the modulation of the EGFR signaling, the Wnt/β-catenin pathway and apoptotic regulation, with ERBB2, CTNNB1, HSP90AA1 and HDAC6 emerging as the main targets. Molecular docking results were consistent with these predictions, with ellagic acid and quercetin showing the most favorable predicted interaction profiles toward ERBB2 and HSP90AA1.

Overall, results indicate that *E. parviflorum* extracts, particularly E3 and E1, may be regarded as promising sources of bioactive compounds with antiproliferative, and pro-apoptotic properties. However, further studies are needed in order to fully correlate the phytochemical profile of the extracts with their biological activity and further confirm the underlying mechanisms. Future investigations should also involve standardized extracts, isolated compounds and more complex experimental models, including in vivo tumor models, in order to validate the cytotoxic activity of *E. parviflorum*.

Author Contributions: Conceptualization, C.G. and R.R.; software, A.P.; validation, C.G. and R.R.; methodology, C,Ș.; investigation, M.J., O.B. and G.A.; data curation, A.M.; writing—original draft preparation, C.G., R.R., M.J., R.N.-G., A.P., O.B. and G.A.; writing—review and editing, C.Ș. and A.M.; funding acquisition, R.N.-G. and A.M. All authors have read and agreed to the published version of the manuscript.

Funding: This work was supported by the Romanian National Authority for Scientific Research through the project UEFISCDI PN-IV-P2-2.1-TE-2023-1790 and PN-IV-P2-2.1-TE-2023-0717. We would like to acknowledge the "Victor Babes" University of Medicine and Pharmacy Timisoara for their support in covering the costs of publication for this research paper.

Institutional Review Board Statement: Not applicable.

Informed Consent Statement: Not applicable.

Data Availability Statement: The original contributions presented in this study are included in the article. Further inquiries can be directed to the corresponding author.

Conflicts of Interest: The authors declare no conflicts of interest.

References

1. Schnaiter, N. Pharmacology of Cancer Drugs: Mechanisms and Applications. *J. Cancer Sci. Res.* **2024**, *9*, 579. [CrossRef]
2. Hartmann, J.T.; Haap, M.; Kopp, H.-G.; Lipp, H.-P. Tyrosine Kinase Inhibitors—A Review on Pharmacology, Metabolism and Side Effects. *Curr. Drug Metab.* **2009**, *10*, 470–481. [CrossRef] [PubMed]

3. Anand, U.; Dey, A.; Chandel, A.K.S.; Sanyal, R.; Mishra, A.; Pandey, D.K.; De Falco, V.; Upadhyay, A.; Kandimalla, R.; Chaudhary, A.; et al. Cancer Chemotherapy and beyond: Current Status, Drug Candidates, Associated Risks and Progress in Targeted Therapeutics. *Genes Dis.* **2023**, *10*, 1367–1401. Correction in *Genes Dis.* **2024**, *11*, 101211. https://doi.org/10.1016/j.gendis.2024.101211. [CrossRef] [PubMed]
4. Cortelo, P.C.; Demarque, D.P.; Dusi, R.G.; Albernaz, L.C.; Braz-Filho, R.; Goncharova, E.I.; Bokesch, H.R.; Gustafson, K.R.; Beutler, J.A.; Espindola, L.S. A Molecular Networking Strategy: High-Throughput Screening and Chemical Analysis of Brazilian Cerrado Plant Extracts against Cancer Cells. *Cells* **2021**, *10*, 691. [CrossRef] [PubMed]
5. Dimitrova, M.; Sulikovska, I.; Tsvetanova, E.; Djeliova, V.; Vasileva, A.; Ivanov, I. Chemical Composition and Biological Activity of Extracts from the Aerial Parts of Epilobium Parviflorum Schreb. *Appl. Sci.* **2025**, *15*, 12109. [CrossRef]
6. Kyriakou, S.; Tragkola, V.; Paraskevaidis, I.; Plioukas, M.; Trafalis, D.T.; Franco, R.; Pappa, A.; Panayiotidis, M.I. Chemical Characterization and Biological Evaluation of Epilobium Parviflorum Extracts in an In Vitro Model of Human Malignant Melanoma. *Plants* **2023**, *12*, 1590. [CrossRef] [PubMed]
7. Lewandowska, K.; Majewski, M.S. The Involvement of Epilobium Parviflorum in Different Human Diseases, with Particular Attention to Its Antioxidant and Anti-Inflammatory Properties and Benefits to Vascular Health. *Nutrients* **2025**, *17*, 1577. [CrossRef] [PubMed]
8. Șachir, E.E.; Pușcașu, C.G.; Caraiane, A.; Raftu, G.; Badea, F.C.; Mociu, M.; Albu, C.M.; Sachelarie, L.; Liliana Hurjui, L.; Bartok-Nicolae, C. Studies Regarding the Antibacterial Effect of Plant Extracts Obtained from Epilobium Parviflorum Schreb. *Appl. Sci.* **2022**, *12*, 2751. [CrossRef]
9. Stolarczyk, M.; Naruszewicz, M.; Kiss, A.K. Extracts from Epilobium Sp. Herbs Induce Apoptosis in Human Hormone-Dependent Prostate Cancer Cells by Activating the Mitochondrial Pathway. *J. Pharm. Pharmacol.* **2013**, *65*, 1044–1054. [CrossRef] [PubMed]
10. Akbudak, M.A.; Sut, T.; Eruygur, N.; Akinci, E. Antiproliferative Effect of Epilobium Parviflorum Extracts on Colorectal Cancer Cell Line HT-29. *Rom. Biotechnol. Lett.* **2021**, *26*, 3120–3128. [CrossRef]
11. Kia, B.H.; Kazemi Noureini, S.; Reza, M.; Kakhki, V.; Noureini, S.K. The Extracts of Epilobium Parviflorum Inhibit MCF-7 Breast Cancer Cells. *Iran. J. Toxicol.* **2021**, *15*, 65–72. [CrossRef]
12. Banc, R.; Rusu, M.E.; Filip, L.; Popa, D.S. The Impact of Ellagitannins and Their Metabolites through Gut Microbiome on the Gut Health and Brain Wellness within the Gut–Brain Axis. *Foods* **2023**, *12*, 270. [CrossRef] [PubMed]
13. Lyubitelev, A.; Studitsky, V. Inhibition of Cancer Development by Natural Plant Polyphenols: Molecular Mechanisms. *Int. J. Mol. Sci.* **2023**, *24*, 10663. [CrossRef] [PubMed]
14. Bray, F.; Laversanne, M.; Sung, H.; Ferlay, J.; Siegel, R.L.; Soerjomataram, I.; Jemal, A. Global Cancer Statistics 2022: GLOBOCAN Estimates of Incidence and Mortality Worldwide for 36 Cancers in 185 Countries. *CA Cancer J. Clin.* **2024**, *74*, 229–263. [CrossRef] [PubMed]
15. Ghiulai, R.; Avram, S.; Stoian, D.; Pavel, I.Z.; Coricovac, D.; Oprean, C.; Vlase, L.; Farcas, C.; Mioc, M.; Minda, D.; et al. Lemon Balm Extracts Prevent Breast Cancer Progression In Vitro and In Ovo on Chorioallantoic Membrane Assay. *Evid.-Based Complement. Altern. Med.* **2020**, *2020*, 6489159. [CrossRef] [PubMed]
16. Oniga, I.; Pus, C.; Silaghi-Dumitrescu, R.; Olah, N.K.; Sevastre, B.; Marica, R.; Marcus, I.; Sevastre-Berghian, A.C.; Benedec, D.; Pop, C.E.; et al. *Origanum vulgare* ssp. Vulgare: Chemical Composition and Biological Studies. *Molecules* **2018**, *23*, 2077. [CrossRef] [PubMed]
17. Roșca, O.J.; Coneac, G.H.; Racoviceanu, R.; Nistor, A.; Olariu, I.V.; Cotan, A.M.; Negrea-Ghiulai, R.; Dehelean, C.A.; Vlaia, L.L.; Șoica, C.M. Optimizing Burn Wound Healing: The Critical Role of PH and Rheological Behavior in Plant-Derived Topical Formulations. *Pharmaceutics* **2025**, *17*, 853. [CrossRef] [PubMed]
18. Zhang, L.; Chen, J.; Wang, Y.; Wu, D.; Xu, M. Phenolic Extracts from Acacia Mangium Bark and Their Antioxidant Activities. *Molecules* **2010**, *15*, 3567–3577. [CrossRef] [PubMed]
19. Chang, C.-C.; Yang, M.-H.; Wen, H.-M.; Chern, J.-C.; Chang, C.-C.; Yang, M.-H.; Wen, H.-M.; Chern, J.-C. Estimation of Total Flavonoid Content in Propolis by Two Complementary Colometric Methods. *J. Food Drug Anal.* **2020**, *10*, 3. [CrossRef]
20. Broadhurst, R.B.; Jones, W.T. Analysis of Condensed Tannins Using Acidified Vanillin. *J. Sci. Food Agric.* **1978**, *29*, 788–794. [CrossRef]
21. Géorcelin, A.G.; Akin, Y.; Lessé, P.D.A.; Challaton, K.P.; Konmy, B.; Valère, S.; Kifouly, H.; Djeho, C.; Olounladé, P.; Hounzangbé-Adoté, S. Effects of Agro-Ecological Origin and Harvest Time of Three Medicinal Plants on Their Anthelmintic Efficacy. *Sci. Rep.* **2026**, *16*, 3980. [CrossRef] [PubMed]
22. Munteanu, A.; Gogulescu, A.; Șoica, C.; Mioc, A.; Mioc, M.; Milan, A.; Lukinich-Gruia, A.T.; Pricop, M.-A.; Jianu, C.; Banciu, C.; et al. In Vitro and In Silico Evaluation of *Syzygium aromaticum* Essential Oil: Effects on Mitochondrial Function and Cytotoxic Potential Against Cancer Cells. *Plants* **2024**, *13*, 3443. [CrossRef] [PubMed]
23. Stelzer, G.; Rosen, N.; Plaschkes, I.; Zimmerman, S.; Twik, M.; Fishilevich, S.; Iny Stein, T.; Nudel, R.; Lieder, I.; Mazor, Y.; et al. The GeneCards Suite: From Gene Data Mining to Disease Genome Sequence Analyses. *Curr. Protoc. Bioinform.* **2016**, *54*, 1.30.1–1.30.33. [CrossRef] [PubMed]

24. The UniProt Consortium. UniProt: The Universal Protein Knowledgebase in 2025. *Nucleic Acids Res.* **2025**, *53*, D609–D617. [CrossRef] [PubMed]
25. Nakanishi, K.; Hato, T.; Imai, A.; Kaneko, H.; Murakami, A.; Kuwashima, K.; Ikeda, K.; Fujita, S.; Kobayashi, Y.; Kaido, H.; et al. Platelet Cyclo-Oxygenase Deficiency in a Japanese. *Scand. J. Haematol.* **1984**, *32*, 167–174. [CrossRef] [PubMed]
26. Manley, R.S.J.; Jonker, J.W.; Cooper, D.; Pound, T.C. Initiation of Cellulose Biosynthesis. *Nat. New Biol.* **1971**, *229*, 88–89. [CrossRef] [PubMed]
27. Brennan, M. Prenatal Administration of Fluorides. *Bull. N. J. Soc. Dent. Child.* **1971**, *18*, 7–11. [PubMed]
28. Kurtz, W. Editorial. Valid Complaint Is the Patient's Right. *Dent. Surv.* **1971**, *47*, 32–33. [PubMed]
29. Ebisu, S.; Kato, K.; Kotani, S.; Misaki, A. Isolation and Purification of Flavobacterium Alpha-1,3-Glucanase-Hydrolyzing, Insoluble, Sticky Glucan of Streptococcus Mutans. *J. Bacteriol.* **1975**, *124*, 1489–1501. [CrossRef] [PubMed]
30. Kim, S.; Chen, J.; Cheng, T.; Gindulyte, A.; He, J.; He, S.; Li, Q.; Shoemaker, B.A.; Thiessen, P.A.; Yu, B.; et al. PubChem in 2021: New Data Content and Improved Web Interfaces. *Nucleic Acids Res.* **2021**, *49*, D1388–D1395. [CrossRef] [PubMed]
31. Hanwell, M.D.; Curtis, D.E.; Lonie, D.C.; Vandermeerschd, T.; Zurek, E.; Hutchison, G.R. Avogadro: An Advanced Semantic Chemical Editor, Visualization, and Analysis Platform. *J. Cheminform.* **2012**, *4*, 17. [CrossRef] [PubMed]
32. Wang, X.; Shen, Y.; Wang, S.; Li, S.; Zhang, W.; Liu, X.; Lai, L.; Pei, J.; Li, H. PharmMapper 2017 Update: A Web Server for Potential Drug Target Identification with a Comprehensive Target Pharmacophore Database. *Nucleic Acids Res.* **2017**, *45*, W356–W360. [CrossRef] [PubMed]
33. Heberle, H.; Meirelles, V.G.; da Silva, F.R.; Telles, G.P.; Minghim, R. InteractiVenn: A Web-Based Tool for the Analysis of Sets through Venn Diagrams. *BMC Bioinform.* **2015**, *16*, 169. [CrossRef] [PubMed]
34. Szklarczyk, D.; Nastou, K.; Koutrouli, M.; Kirsch, R.; Mehryary, F.; Hachilif, R.; Hu, D.; Peluso, M.E.; Huang, Q.; Fang, T.; et al. The STRING Database in 2025: Protein Networks with Directionality of Regulation. *Nucleic Acids Res.* **2025**, *53*, D730–D737. [CrossRef] [PubMed]
35. Shannon, P.; Markiel, A.; Ozier, O.; Baliga, N.S.; Wang, J.T.; Ramage, D.; Amin, N.; Schwikowski, B.; Ideker, T. Cytoscape: A Software Environment for Integrated Models of Biomolecular Interaction Networks. *Genome Res.* **2003**, *13*, 2498. [CrossRef] [PubMed]
36. Zhou, Y.; Zhou, B.; Pache, L.; Chang, M.; Khodabakhshi, A.H.; Tanaseichuk, O.; Benner, C.; Chanda, S.K. Metascape Provides a Biologist-Oriented Resource for the Analysis of Systems-Level Datasets. *Nat. Commun.* **2019**, *10*, 1523. [CrossRef] [PubMed]
37. Tóth, B.H.; Blazics, B.; Kéry, Á. Polyphenol composition and antioxidant capacity of Epilobium species. *J. Pharm. Biomed. Anal.* **2009**, *49*, 26–31. [CrossRef] [PubMed]
38. Platzer, M.; Kiese, S.; Herfellner, T.; Schweiggert-Weisz, U.; Eisner, P. How Does the Phenol Structure Influence the Results of the Folin-Ciocalteu Assay? *Antioxidants* **2021**, *10*, 811. [CrossRef] [PubMed]
39. Merighi, S.; Travagli, A.; Tedeschi, P.; Marchetti, N.; Gessi, S. Antioxidant and Antiinflammatory Effects of Epilobium Parviflorum, Melilotus Officinalis and Cardiospermum Halicacabum Plant Extracts in Macrophage and Microglial Cells. *Cells* **2021**, *10*, 2691. [CrossRef] [PubMed]
40. Sun, B.; Ricardo-da-Silva, J.M.; Spranger, I. Critical Factors of Vanillin Assay for Catechins and Proanthocyanidins. *J. Agric. Food Chem.* **1998**, *46*, 4267–4274. [CrossRef]
41. Karakaya, S.; Suntar, I.; Aydin, B.; Dursunoglu, B.; Gözcu, S.; Senol, O.; Bayrak, B.; Ozbek, H.; Koca, M.; Ceribasi, S.; et al. Evaluation of Anticholinesterase Effect of Some Epilobium Species and Quantification of Hyperoside by HPLC. *Nat. Prod. Res.* **2020**, *36*, 1296–1299. [CrossRef] [PubMed]
42. Vlase, A.M.; Toiu, A.; Tomuță, I.; Vlase, L.; Muntean, D.; Casian, T.; Fizeșan, I.; Nadăș, G.C.; Novac, C.Ș.; Tămaș, M.; et al. Epilobium Species: From Optimization of the Extraction Process to Evaluation of Biological Properties. *Antioxidants* **2022**, *12*, 91. [CrossRef] [PubMed]
43. Mohammadi Bazargani, M.; Falahati-Anbaran, M.; Rohloff, J. Comparative Analyses of Phytochemical Variation Within and Between Congeneric Species of Willow Herb, Epilobium Hirsutum and E. Parviflorum: Contribution of Environmental Factors. *Front. Plant Sci.* **2021**, *11*, 595190. [CrossRef] [PubMed]
44. Qiu, J.; Zhang, T.; Zhu, X.; Yang, C.; Wang, Y.; Zhou, N.; Ju, B.; Zhou, T.; Deng, G.; Qiu, C. Hyperoside Induces Breast Cancer Cells Apoptosis via ROS-Mediated NF-KB Signaling Pathway. *Int. J. Mol. Sci.* **2019**, *21*, 131. [CrossRef] [PubMed]
45. Zhu, M.L.; Zhang, P.M.; Jiang, M.; Yu, S.W.; Wang, L. Myricetin Induces Apoptosis and Autophagy by Inhibiting PI3K/Akt/MTOR Signalling in Human Colon Cancer Cells. *BMC Complement. Med. Ther.* **2020**, *20*, 209. [CrossRef] [PubMed]
46. Feng, G.; Zhang, L.; Bao, W.; Ni, J.; Wang, Y.; Huang, Y.; Lyv, J.; Cao, X.; Chen, T.; You, K.; et al. Gentisic Acid Prevents Colorectal Cancer Metastasis via Blocking GPR81-Mediated DEPDC5 Degradation. *Phytomedicine* **2024**, *129*, 155615. [CrossRef] [PubMed]
47. Cincin, Z.B.; Unlu, M.; Kiran, B.; Bireller, E.S.; Baran, Y.; Cakmakoglu, B. Apoptotic Effects of Quercitrin on DLD-1 Colon Cancer Cell Line. *Pathol. Oncol. Res.* **2014**, *21*, 333–338. [CrossRef] [PubMed]

48. Liu, Q.; Liu, F.; Zhang, L.; Niu, Y.; Liu, Z.; Liu, X. Comparison of Chicoric Acid, and Its Metabolites Caffeic Acid and Caftaric Acid: In Vitro Protection of Biological Macromolecules and Inflammatory Responses in BV2 Microglial Cells. *Food Sci. Hum. Wellness* **2017**, *6*, 155–166. [CrossRef]
49. Farina, A.; Tartaglione, S.; Preziosi, A.; Mancini, P.; Angeloni, A.; Anastasi, E. PANC-1 Cell Line as an Experimental Model for Characterizing PIVKA-II Production, Distribution, and Molecular Mechanisms Leading to Protein Release in PDAC. *Int. J. Mol. Sci.* **2024**, *25*, 3498. [CrossRef] [PubMed]
50. Fernandez, M.F.; Charfi, C.; Piloto-Ferrer, J.; González, M.L.; Lamy, S.; Annabi, B. Targeting Ovarian Cancer Cell Cytotoxic Drug Resistance Phenotype with *Xanthium strumarium* L. Extract. *Evid.-Based Complement. Altern. Med.* **2019**, *2019*, 6073019. [CrossRef] [PubMed]
51. Reyes-Castellanos, G.; Masoud, R.; Carrier, A. Mitochondrial Metabolism in PDAC: From Better Knowledge to New Targeting Strategies. *Biomedicines* **2020**, *8*, 270. [CrossRef] [PubMed]
52. Saraste, A.; Pulkki, K. Morphologic and Biochemical Hallmarks of Apoptosis. *Cardiovasc. Res.* **2000**, *45*, 528–537. [CrossRef] [PubMed]
53. Yang, Y.; He, P.Y.; Zhang, Y.; Li, N. Natural Products Targeting the Mitochondria in Cancers. *Molecules* **2020**, *26*, 92. [CrossRef] [PubMed]
54. Noor, F.; Qamar, M.T.U.; Ashfaq, U.A.; Albutti, A.; Alwashmi, A.S.S.; Aljasir, M.A. Network Pharmacology Approach for Medicinal Plants: Review and Assessment. *Pharmaceuticals* **2022**, *15*, 572. [CrossRef] [PubMed]
55. Liu, J.; Meng, J.; Li, R.; Jiang, H.; Fu, L.; Xu, T.; Zhu, G.Y.; Zhang, W.; Gao, J.; Jiang, Z.H.; et al. Integrated Network Pharmacology Analysis, Molecular Docking, LC-MS Analysis and Bioassays Revealed the Potential Active Ingredients and Underlying Mechanism of Scutellariae Radix for COVID-19. *Front. Plant Sci.* **2022**, *13*, 988655. [CrossRef] [PubMed]
56. Zhang, C.; Liu, C.; Qu, Y.; Cao, Y.; Liu, R.; Sun, Y.; Nyima, T.; Zhang, S.; Sun, Y. LC–MS-Based Qualitative Analysis and Pharmacokinetic Integration Network Pharmacology Strategy Reveals the Mechanism of Phlomis Brevidentata H.W.Li Treatment of Pneumonia. *ACS Omega* **2021**, *6*, 4495–4505. [CrossRef] [PubMed]
57. Yagi, S.; Cetiz, M.V.; Zengin, G.; Llorent-Martínez, E.J.; Yıldıztugay, E.; Bingol, Z.; Gulcin, I.; Dall'Acqua, S. A Thorough Exploration of the Chemical Profile and Biological Potential of Epilobium Parviflorum Extracts Using HPLC-ESI-Q-TOF-MS Technique along with in Vitro and in Silico Analysis. *J. Agric. Food Res.* **2025**, *24*, 102414. [CrossRef]
58. Crespy, V.; Morand, C.; Besson, C.; Manach, C.; Démigné, C.; Rémésy, C. Comparison of the Intestinal Absorption of Quercetin, Phloretin and Their Glucosides in Rats. *J. Nutr.* **2001**, *131*, 2109–2114. [CrossRef] [PubMed]
59. Ji, L.; Shi, W.; Li, Y.; He, J.; Xu, G.; Qin, M.; Guo, Y.; Ma, Q. Systematic Identification, Fragmentation Pattern, And Metabolic Pathways of Hyperoside in Rat Plasma, Urine, And Feces by UPLC-Q-Exactive Orbitrap MS. *J. Anal. Methods Chem.* **2022**, *2022*, 2623018. [CrossRef] [PubMed]
60. Jensen, J.D.; Dunn, J.H.; Luo, Y.; Liu, W.; Fujita, M.; Dellavalle, R.P. Ellagic Acid Inhibits Melanoma Growth in Vitro. *Dermatol. Rep.* **2011**, *3*, e36. [CrossRef] [PubMed]
61. Roman, A.; Smeu, A.; Lascu, A.; Dehelean, C.A.; Predescu, I.-A.; Motoc, A.; Borza, C.; Draghici, G.A.; Trandafirescu, C.M.; Anton, A.; et al. Quercetin Enhances 5-Fluorouracil-Driven Cytotoxicity Dose-Dependently in A375 Human Melanoma Cells. *Life* **2024**, *14*, 1685. [CrossRef] [PubMed]
62. Khan, R.U.Z.; Yanase, E.; Trivedi, V. Extraction, phytochemical characterization and anti-cancer mechanism of Haritaki churna: An ayurvedic formulation. *PLoS ONE* **2023**, *18*, e0286274. [CrossRef] [PubMed]
63. Cheng, H.; Lu, C.; Tang, R.; Pan, Y.; Bao, S.; Qiu, Y.; Xie, M. Ellagic acid inhibits the proliferation of human pancreatic carcinoma PANC-1 cells *in vitro* and *in vivo*. *Oncotarget* **2017**, *8*, 12301–12310. [CrossRef] [PubMed]
64. Qian, X.; Bi, Q.-Y.; Wang, Z.-N.; Han, F.; Liu, L.-M.; Song, L.-B.; Li, C.-Y.; Zhang, A.-Q.; Ji, X.-M. Qingyihuaji Formula promotes apoptosis and autophagy through inhibition of MAPK/ERK and PI3K/Akt/mTOR signaling pathway on pancreatic cancer in vivo and in vitro. *J. Ethnopharmacol.* **2023**, *307*, 116198. [CrossRef] [PubMed]
65. Elsaid, F.G.; Alshehri, M.A.; Shati, A.A.; Al-Kahtani, M.A.; Alsheri, A.S.; Massoud, E.E.; El-Kott, A.F.; El-Mekkawy, H.I.; Al-Ramlawy, A.M.; Abdraboh, M.E. The anti-tumourigenic effect of ellagic acid in SKOV-3 ovarian cancer cells entails activation of autophagy mediated by inhibiting Akt and activating AMPK. *Clin. Exp. Pharmacol. Physiol.* **2020**, *47*, 1611–1621. [CrossRef] [PubMed]
66. Xu, G.; Li, B.; Wang, T.; Wan, J.; Zhang, Y.; Huang, J.; Shen, Y. Enhancing the anti-ovarian cancer activity of quercetin using a self-assembling micelle and thermosensitive hydrogel drug delivery system. *RSC Adv.* **2018**, *9*, 21229–21242. Correction in *RSC Adv.* **2019**, *9*, 33193–33194. https://doi.org/10.1039/c9ra90071c. [CrossRef] [PubMed]
67. Sukniam, K.; Manaise, H.K.; Popp, K.; Popp, R.; Gabriel, E. Role of Surgery in Metastatic Melanoma and Review of Melanoma Molecular Characteristics. *Cells* **2024**, *13*, 465. [CrossRef] [PubMed]

68. Shang, Y.; Cao, T.; Li, J.; Li, J.; Zhang, L.; Ma, Q.; Feng, L.; Zhao, H. BRAF inhibitor resistance in melanoma: From resistance mechanisms to therapeutic innovations. *Mol. Biomed.* **2026**, *7*, 27. [CrossRef] [PubMed]
69. Wang, F.; Chen, J.; Xiang, D.; Lian, X.; Wu, C.; Quan, J. Ellagic acid inhibits cell proliferation, migration, and invasion in melanoma via EGFR pathway. *Am. J. Transl. Res.* **2020**, *12*, 2295–2304. [PubMed]